Fermilab

Fermi National Accelerator Laboratory
P.O. Box 500 • Batavia, Illinois • 60510

ANTIPROTON-PROTON COLLIDER UPGRADE: LINAC

CONCEPTUAL DESIGN

REVISION 1

FEBRUARY, 1988

OPERATED BY UNIVERSITIES RESEARCH ASSOCIATION, INC.
FOR THE UNITED STATES DEPARTMENT OF ENERGY

Preface

This is Revision I of the Conceptual Design of the Antiproton-Proton Collider Upgrade-Linac dated February, 1988. This Revision supersedes the April, 1987 version of the same document which was entitled Tevatron Upgrade-Linac. Minor changes have been made in this revision of the 1987 Conceptual Design report mainly to reflect the R&D effort that has been done in the past year. For example:

- Greater mention is made of the Disk-and-Washer and the Side-Coupled accelerating structure prototypes which are being constructed to verify the higher accelerating gradients required in the Upgrade.

- Further iteration of the reference design has been done to reflect the many SUPERFISH computer runs made to study the structure properties and studies of a detailed transverse focusing scheme.

- More detailed beam dynamics studies have been done to verify the improvement in the beam properties.

- The peak power requirement on the klystron power supply has been increased from 10 MW to 12 MW to allow a larger margin for losses in the coupling cells, bridge couplers, and phase-amplitude control system.

- The cost estimate has been updated to account for the above changes, 1987 inflation, and revised escalation factors.

- The master schedule has been revised to reflect the start of construction in FY-90.

It is the opinion of the editors of this report that this revision will clarify some issues which were not adequately addressed in the earlier version. The conceptual design describes herein has been advanced toward a more detailed design.

Antiproton-Proton Collider Upgrade-Linac

Table of Contents

Antiproton-Proton Collider Upgrade-Linac

I. Introduction

The goal of the Antiproton-Proton Collider Upgrade program is to achieve an improvement in the Collider luminosity and the fixed-target intensity. The Linac portion of this project will increase the energy of the existing 200-MeV linac to 400 MeV in order to reduce beam emittance degradation in the Booster.

The critical parameters which limit the luminosity of the Tevatron Collider are the beam emittances, both longitudinal and transverse, at each stage in the acceleration sequence. Critical limitations occur because the beam emittance grows significantly during the first few milliseconds after injection into the Booster, during acceleration through transition in the Booster, at injection into the Main Ring, during acceleration through transition in the Main Ring, during rf bunch manipulation in the Main Ring, and finally, during injection into the Tevatron. Improvements are underway to significantly reduce the emittance growth which occurs in the Booster at transition and in all stages of Main Ring operation. The suspected cause of the emittance growth during the first few milliseconds after injection into the Booster is due to the tune spread caused by space charge and small errors in the magnetic guide field. The most practical way to eliminate this growth is to increase the energy of the Linac, thereby reducing the tune spread due to space charge. The increase in energy will not only help provide a smaller emittance beam for Collider operation, it will help provide higher intensity beams for fixed target operation.

By increasing the Linac energy from 200 MeV to 400 MeV, the phase space density limitation (defined by the ratio of the number of particles to the beam emittance) a few milliseconds after injection into the Booster can be increased by about 1 3/4 times. Since the initial beam emittance will be smaller, the beam size will be smaller, and the effects of nonlinear field errors on emittance growth will be smaller. Further, at the higher magnetic guide field needed at 400 MeV, the strengths of the remanent and eddy current field errors will be proportionately smaller. The rf capture of the injected beam will be improved because of the larger ratio of

available bucket area to beam phase space area. These factors will make possible a more intense beam with a smaller emittance. A more detailed discussion of the effect of the linac upgrade on Booster performance appears in Section II.

The Fermilab 200-MeV linac was designed in the late 1960's. A number of advances in linac technology have been made since that time including the ability to achieve higher accelerating gradients. In addition, more efficient rf power sources are available. (A particular difficulty of the present Alvarez linacs operating at a frequency of 200 MHz is the availability of the final power amplifier tube which is obsolete. Replacements must be obtained by rebuilding tubes that have already failed in service.) The question of changing from the Alvarez drift-tube structure to a more efficient structure above 100 MeV was discussed at the time of construction of the Fermilab linac. For the sake of replication of components and simplicity, it was decided to continue the drift-tube structure to 200 MeV even though the side-coupled structure was known to be more efficient at higher energies. It seems reasonable now to consider replacing the higher energy cavities with more efficient accelerating structures operating at a higher gradient and thus increase the energy of the linac in the same available building space.

R and D, not related to this project, is currently underway to understand the growth in beam emittance that occurs between the ion source and the entrance to the linac. It is possible that this R and D will result in system improvements, such as the addition of a radio-frequency quadrupole (RFQ) structure between the ion source and the linac. The benefits of improving the beam quality at low energy in the system will allow the transition to a new structure at higher energy to be made easier, but will not change the design proposed in this report.

The Linac upgrade project provides for the replacement of the last four Linac cavities with more efficient, higher accelerating gradient cavities. The last four drift tube cavities, from 116 MeV to 200 MeV, will be replaced with seven side-coupled cavities operating at a frequency of 805 MHz, four times the operating frequency of the present Linac cavities. The higher frequency side-coupled cavity structure is physically smaller, is constructed of single cells brazed together in a structure capable of high vacuum,

and can be operated reliably at much higher accelerating gradients, i.e., 7.5 MV/m compared to 2.5 MV/m in the drift-tube structure. These seven side-coupled cavity modules, installed in the space made available by replacing the four drift-tube tanks and driven by seven 12 MW, 805 MHz klystron rf power supplies, will accelerate the beam from 116 MeV to 400 MeV. In addition, a special matching section will be added between the drift-tube and side coupled cavity structures to allow a proper match between these different Linac structures. The present injection and transport line to the Booster accelerator will be modified by replacing a few elements to accommodate the higher energy. A complete discussion of these aspects of the Linac Upgrade appears in Section III.

II. Impact of a 400-MeV Linac on Booster Performance

With the advent of the proton-antiproton collider at Fermilab a change has taken place in the criteria by which performance of the Booster and Main Ring accelerators are judged. For both collider and fixed target operation the normal figure of merit is the luminosity, which is the proportionality constant between the interaction rate observed by an experimenter and the cross section for a particular process. In the collider mode of operation, luminosity depends directly on the density of particles (i.e. particles per transverse phase space) circulating in the Tevatron, while for fixed target physics the luminosity depends only on the total number of particles extracted from the Tevatron. Thus in the collider era Booster performance is no longer judged simply by how many protons can be accelerated, but by what density of particles can be delivered. This distinction is important because it determines the strategy followed in attempting to upgrade the Booster performance. As we will show below, we have evidence that the beam density in the Booster is limited by incoherent space-charge effects at injection, while the total beam intensity is limited by the combination of space-charge and aperture. As we will further discuss below, the fundamental space-charge limitation can best be dealt with by raising the Booster injection energy.

Current Booster performance is summarized in Figures 1 and 2. The figures are based on measurements completed during the August 1986 startup and following the spring, 1987, Collider run. In Figure 1 the total amount of beam which can be accelerated in the Booster is

plotted as a function of the number of injected turns. The Booster uses a multiple turn injection scheme in which H^- ions coming out of the Linac are stripped to form H^+ by passing through a thin foil. This injection procedure allows us to run up to 3.5×10^{12} particles in the Booster while only using 5×10^{11} particles per injected turn from the Linac (operating at 30mA). We see from Figure 1 that at low-to-moderate intensities the number of protons accelerated in the Booster increases almost linearly with the number of injected turns, while at high intensities it becomes impossible to accelerate more than about 3.5×10^{12} protons, independent of the number of injected particles.

An understanding of this limitation can be gained by looking at Figure 2 where we have plotted the normalized transverse emittance of the extracted Booster beam (i.e. the beam size) as a function of the number of protons accelerated. In the figure we have displayed both the vertical and horizontal emittances.* In principle, we might expect to be able to increase the phase space density of the beam to an arbitrarily large value because the multiple turn H^- injection allows us to lay subsequent turns exactly on top of each other. Figure 2 shows that this is not so. At low intensities, up to about 1.2×10^{12}, the extracted beam size is independent of the number of protons, that is the phase space density is increasing with the number of injected turns. However, at higher intensities the beam size starts to grow following the dashed line on the figure. The dashed curve is close to a contour of constant phase space density. It says that we are not able to achieve a density of more than $1.7 \times 10^{12}/10\pi$ mm-mr total or $2.0 \times 10^{10}/10\pi$ mm-mr/bunch in the Booster. This is about a factor of two lower than that proposed for the Collider Upgrade.

The two figures present a self-consistent picture of what is going on in the present Booster: The Booster beam size is just what is delivered from the Linac as long as this does not produce a density higher than the limit cited above. At higher intensities the beam size blows up in such a way as to keep the phase space density at the

*The momentum spread in the beam is also displayed. Momentum spread and horizontal transverse emittance have been separately determined through measurements taken at points with similar beta functions but different dispersions.

prescribed limit. The limit on the total amount of beam which can be accelerated is reached when the beam size gets big enough to fill the available aperture.

As stated earlier we believe the observed limit on the charge density that can be produced in the Booster arises from the incoherent space-charge tune shift at injection. The physical mechanism is as follows: A proton located within a bunch in the Booster is subject to both electric and magnetic forces due to other protons within the same bunch. Since these forces depend on the transverse position of the proton, they provide additional focussing which changes the tune of a particle in a manner which depends on its oscillation amplitude. As a result an incoherent tune spread is introduced in the beam whose magnitude is given by[1]

$$\Delta\nu_{s.c.} = \frac{3r_pN_t}{2B\beta\gamma^2\epsilon_N} \qquad (1)$$

where r_p is the classical radius of the proton, N_t is the total number of particles in the accelerator, B is the ratio of average to peak current, β and γ are the usual kinematic factors, and ϵ_N is the normalized (95%) transverse emittance.* The kinematic dependence on β and γ arises because the electric and magnetic field contributions exactly cancel as β goes to 1. The strong kinematic dependence insures that in any accelerator complex the total tune spread within the beam is apt to be largest at injection into the lowest energy ring. The mechanism by which the incoherent tune spread limits beam intensity is presumably by restricting the tunes to lie in a resonance free region. One would expect that the best one could possibly hope to do would be to run with a space-charge tune spread of 0.5. In practice one might expect to be even more restricted. Examination of the above expression shows that for fixed kinematics the tune spread is proportional to the phase space density of the beam. The dashed lines shown in Figure 2 represent contours of constant space-charge tune spread ($\Delta\nu_{s.c.} = 0.38$). We believe that the above described mechanism is providing a fundamental limit on the beam density which we can achieve in the Booster. Two additional observations lend further credence to this hypothesis. First, we have looked at beam profiles throughout the Booster acceleration cycle and have found that to within our measurement resolution (1.5msec) the blowup seen at high intensity occurs at injection. Second, we have observed incoherent

*The formula is modified slightly if horizontal and vertical emittances are unequal and/or the momentum spread is non-zero.

resonance lines early in the acceleration cycle and have seen them broaden as the beam intensity is raised. These observations are in qualitative agreement with what we expect from the above described mechanism.

Given that we believe that the incoherent space-charge tune spread is providing the fundamental limit on the achievable beam density in the Booster, it is clear from the space-charge tune spread formula that the only good way to raise the phase space density of the beam delivered out of the Booster is to raise the injection energy. The only other options available, other than building a ring with a smaller circumference, are to increase the bunching factor during the initial stages of acceleration or to correct enough resonances to allow one to approach space-charge tune spreads of 0.5. Although we are currently experimenting with both of these options, it is unlikely that gains of greater than 10-20% can be achieved in these ways. Increasing the Linac energy from 200 MeV to 400 MeV increases the kinematic factor, $\beta\gamma^2$, in the denominator of (1) from .83 to 1.45. This will raise the fundamental limitation on the Booster phase space density by about 75%.

Below we summarize the expected benefits to the Booster of raising the injected beam energy to 400 MeV, including several effects not included in the above discussion.

1. Increase the achievable phase space density. The achievable phase space density should increase from about 2.0 to about $3.5\text{x}10^{10}/10\pi$ mm-mr/bunch.

2. Increase the total amount of beam deliverable. The effective aperture of the Booster will increase by about 50% in normalized units due to increased adiabatic damping in the linac. Combined with the increased phase space density achievable this, in principle, would allow one to increase the total amount of beam delivered by a factor of 2.6. We don't really expect this to happen because we would expect the increase to be accompanied by other instabilities and difficulties in transmission of the larger beam current in the Main Ring. An increase in total delivered beam of 50%-75% is perhaps reasonable to expect in the long run however.

3. Better field quality at Booster injection. This will come about for two reasons. First, the higher injection fields will reduce the effects of remnant fields in the Booster magnets. And second, the smaller beam size out of the Linac will result in the beam being spread over a region of more uniform field than it is at present. It is hard to quantify the expected benefit from this effect.

4. Improved RF capture. The higher injection energy will result in a larger bucket area during the initial stages of acceleration as well as reducing the frequency swing during the acceleration cycle by about one third. This benefit is also hard to quantify.

III. The Linac Injector Upgrade

A. RF Accelerating Structure

a. Structure Choice

For the purpose of the conceptual design the side-coupled accelerating structure (SCS) has been selected for the region above β=0.456 (116 MeV). The SCS was developed in the early 1960's for use on the LAMPF accelerator where a transition from the drift-tube structure to the SCS was made at 100 MeV. Since then the SCS has been used in many industrial and medical applications for electron and x-ray beams, on the LANL free electron laser for high intensity pulsed electron beams, and as the accelerating section in the racetrack microtrons at the NBS and the University of Illinois.

Other types of accelerating structures (Fig. 3) could be considered and some of these have been studied for use in the LANL/NBS racetrack microtron.[2] SUPERFISH computer runs have been made for the disk and washer (DAW), annular-ring coupled structure (ACS), on-axis coupled structure (OAC), side-coupled structure (SCS), and the coaxial-coupled structure (CCS) at β=.456 (116 MeV). The particular properties considered for the upgrade application, included: (1) a high efficiency (high value of the shunt impedance ZT^2, where Z is the ratio of the square of the accelerating field to the rf power dissipated per length in the structure, and T is the transit time factor) to minimize rf power consumption, (2) an ability to support high accelerating fields, (3) a mode spectrum without

interfering modes close to the fundamental accelerating mode in the structure, (4) good cell-to-cell coupling to ensure good stability with long assemblies of many cells, and (5) good mechanical properties to allow simple fabrication, simplified tuning, and good pumping speed for high vacuum. Table 1 summarizes these preliminary results.

Table 1

Comparison of Shunt Impedance (ZT^2)
for Various Linac Structures
(at β=.456, KE=116 MeV)

Structure	ZT^2 (MΩ/m)	Remarks
DAW	38	Best coupling, best vacuum properties, most interfering modes
SCS	36	Good vacuum, "easy" tuning, coupling only a few % (2-4%)
ACS	36	Poor vacuum, difficult tuning, good coupling. Dipole interfering mode
OAC	25	Poor vacuum, difficult tuning, moderate coupling
CCS	25	Poor vacuum, difficult tuning, good coupling

The DAW structure has been used for the higher energy (100 to 600 MeV) accelerating cavities in the Institute of Nuclear Research meson factory at the USSR Academy of Sciences, Moscow.[3] The USSR experience has been sufficiently positive so that they are developing a design for a DAW accelerating structure to be used in a racetrack microtron.[4] This USSR work has directly confronted the problem of interfering modes which has discouraged the use of the DAW structure in this country. The DAW structure has been considered also for accelerating cavities in the TRISTAN accelerator at the National Laboratory for High Energy Physics, KEK, Japan.[5] The outstanding features of the DAW structure are the high efficiency for rf acceleration, the high stability resulting from the large coupling between cells, and good vacuum properties.

It is necessary to distribute focusing elements along the linac to control the radial extent of the beam so that it passes cleanly through the limiting apertures. The DAW structure adapts to this requirement in a straightforward way that adds little to the length of the accelerator. If the space between two washers is enclosed by a can as shown in Fig. 4, the accelerating field is eliminated from that cell, but the coupling field around the cell is little affected. The resulting enclosure with an outer radius of approximately 17.5 cm and length greater than $\beta\lambda/2$(>8.5 cm at 805 MHz) is sufficient to contain the quadrupole required for a FODO focusing structure with 1 m between quads. Because these coaxial couplers are only one cell long, it is practical to space them every meter, a spacing which limits the maximum beam radius to less than 1 cm. This beam radius in turn allows the choice of an aperture radius of 1.5 cm which results in an improvement in the shunt impedance. The use of rare earth permanent magnet quadrupoles is very attractive for structural simplicity. Beam optics calculations show that focusing requires less than 7 kG pole tip fields for 2 cm radius quads over the full energy range if the entire coupling cell length is used, a value comfortably within current practice. By eliminating power leads and some fraction of the cooling requirement the use of the permanent magnet quads simplifies the radial supports for the coaxial couplers. The simplification helps to limit the support size so that power loss and field perturbation from the coupler are minimized. The very natural way in which the requirements for transverse focusing can be incorporated into the DAW structure add to the attractiveness of this option.

The option of using a DAW accelerating structure shows promise; it is one of the principal focuses of our research and development program. However, at the present time the SCS is better understood and fully proven. From the LANL experience in the construction and operation of LAMPF and the NBS Microtron, we have available the information to demonstrate that our performance goals are reasonable. Cost estimates are based on the LANL experience with SCS as well. Therefore the following reference design employs a SCS derived from that used for the LAMPF linac.

b. Design Assumptions and Criteria

Because the 400-MeV linac is to replace that part of the existing 200 MHz Alvarez linac which accelerates from 116.54 to 200 MeV, it must have a high gradient and make conservative use of space for matching, focusing, mechanical systems etc. The 66 m made available by removing the last four 200 MHz tanks must accommodate a transition section for matching the old and new accelerators, the 400-MeV linac itself, and about 2 m at the downstream end for changes to the Linac-to-Booster transport line. The other major design goals are to minimize power consumption and to keep all parameters within a range favoring dependable routine operation. Table 2 summarizes the principal design criteria and parameters.

Purely from the standpoint of gradient, power economy, power sources, etc. the choice of 805 MHz for the 400-MeV linac is toward the low frequency side of a broad optimum. However, the longitudinal emittance of the beam from the 200 MHz linac is large enough that a larger frequency ratio between structures risks degrading the performance by nonlinearity of the phase-energy oscillations (Section III.C).

In a standing wave linac, the accelerating electric field seen by a synchronous particle is

$$E_z = E_o(z)\ \cos(\omega t+\phi_s) = E_o(z)\ \cos(\omega z/v_s+\phi_s), \tag{2}$$

where $E_o(z)$ is the field amplitude, v_s is the synchronous velocity and ϕ_s is the synchronous phase (determined by longitudinal phase stability). The energy gain per unit cell length by a synchronous particle is

$$\Delta W/L = eE_oT\cos\phi_s, \tag{3}$$

where

$$E_o = \int_{-L/2}^{L/2} E_o(z)dz/L \tag{4}$$

is the average axial accelerating field, and

$$T = \int_{-L/2}^{L/2} E_o(z)\cos(2\pi z/\beta\lambda)dz/E_oL \tag{5}$$

Initial kinetic energy (T_i)	116.54	MeV
Final kinetic energy (T_f)	400.	MeV
Length, including transition section	63.998	m
Frequency of rf (f)	805.0	MHz
Beam current averaged over pulse ($\bar{I}_b$)	50.	mA
Beam pulse length	$< 100.$	μs
Repetition rate	15.0	Hz
Accelerating phase (φ_s)	-32.	deg
Effective accelerating field ($E_0 T cos(\varphi_s)$)	6.3–5.8	MV/m
Maximum surface field (E_{max})	44.	MV/m
Kilpatrick limit (E_K)	26.	MV/m
Number of modules	7	
RF power/module, typical	$< 12.$	MW
copper loss	7.3	MW
beam power	2.1	MW
reserve and control	2.	MW
Number of sections/module	4	
Number of rf cells/section	15	
Total number of rf cells ($7 \times 4 \times 15$)	420	
Length of bridge couplers between sections	$\frac{3}{2}\beta\lambda$	
Transverse focusing scheme	FODO	
Transverse phase advance/FODO cell, average	56.	deg
Quadrupole magnetic length	8.0	cm
Typical quadrupole poletip field	3.4	kG
Quadrupole poletip radius (r_q)	2.0	cm
Beampipe radius (r_p)	1.5	cm

Table 2: Design criteria and general parameters for the 400-MeV SC linac

is the transit time factor which takes into account the temporal variation in the standing wave field as a synchronous particle crosses a cell.

To accelerate the H^- beam from 116 MeV to 400 MeV in the same length as the last four Alvarez tanks requires an average axial field E_o of approximately 7.5 MV/m which is three times the average axial field used in the Alvarez tanks to be replaced. This field is higher than used in any existing proton or H^- linac. However to put this value in perspective requires a criterion for judging high fields. An examination of the constraints of conditioning times, x-ray levels and spark rates suggests that this is an achievable operating gradient at 805 MHz.[6] Since no comprehensive study of maximum operating gradients exists in the literature, only power tests can ultimately determine if reliable operation is possible at this gradient. These three constraints will be experimentally studied using a special SC power test model now under construction (Figure 5).

Long conditioning times to reach a final operating gradient are unacceptable for an injector which other downstream accelerators rely on for beam. Conditioning times seem to be very dependent on vacuum and cavity surface conditions which differ greatly from one accelerator to another. The constraints of x-ray levels and spark rates on the operating gradient are only slightly better understood than conditioning times.

Historically surface breakdown fields under cw conditions have been estimated with the empirical Kilpatrick criterion, established when untrapped oil diffusion vacuum pumps were used.[7] The criterion can be written in the form:

$$f=1.643\ E_k^2\ \exp(-8.5/E_k) \qquad (6)$$

where f is the frequency in MHz, and E_k is the Kilpatrick sparking limit in MV/m. At 805 MHz, E_k is about 26 MV/m. The axial accelerating field E_o in a low energy standing wave structure is some fraction (typically 1/4 to 1/6) of the maximum surface field. For example, a maximum surface field of 45 MV/m ($\simeq 6\ E_o$) for the Linac Upgrade corresponds to approximately 1.7 times the Kilpatrick limit. The present Alvarez linac operates with a maximum surface field of about 1 E_k ($\simeq$ 15 MV/m) at 200 MHz.

Recent experiments report surface breakdown fields of 2 to 8 times the Kilpatrick limit but usually do not specify the spark rate per unit length of structure.[8] The variation in pulse lengths from milliseconds to nanoseconds indicates higher fields can be supported at shorter pulse lengths for a given frequency. For example RFQ experiments[9] show that surface fields of 2.7 E_k can be reached for a 150 μsec pulse length, roughly that for the Linac Upgrade. The spark rate was approximately 1 spark/1000 rf pulses/meter. This corresponds to approximately 1 spark/minute/meter at the 15 Hz repetition rate of the Linac and is certainly unacceptably high for an injector.

The choice of 1.7 E_k for the Linac Upgrade gradient is supported by x-ray emission considerations. Excessive x-ray emission (from field emitted electron bremsstrahlung) both damages beamline organic (e.g. seals, insulation) resulting in significant downtime and drains expensive rf power. Early 200 MHz drift-tube cavity studies at a 15 Hz repetition rate showed that x-ray emission of 400 R/hr occurred for surface fields of 2.7 E_k, while for surface fields of 1.6 E_k x-ray emission was reduced to less than 4 R/hr.[10]

A typical SC structure is illustrated in Figure 6a. Between two accelerating sections is shown an offset rf coupler, called a bridge coupler, which is a suitable place to excite the structure and can be used also to provide space for a focusing quad. To maintain synchronism between the rf and beam particles these couplers must have length equal to an odd multiple of the elementary cell length $\beta\lambda/2$. Here β is the particle velocity divided by the speed of light, and λ is the free space wavelength of the rf. Figure 5 shows a five-cell coupler which is being constructed in a prototype assembly of the SC structure to test operation at full rf excitation.

The rf properties of SCS cells are determined from SUPERFISH calculations. The cell shown in Figure 7 is closely based on LAMPF; the bore radius has been reduced to 1.5 cm from 1.6 cm and the nose cone angle reduced from 30° to 15° to improve the shunt impedance. Cavity dimensions were calculated to maximize shunt impedance for all β. The program SUPERFISH has been used to calculate the transit time factor T, the effective shunt impedance ZT^2 and the peak surface gradient E_{max} at several values of β corresponding to the energy

range 116 to 400 MeV. Because this program is limited to azimuthally symmetric structures, it can not account for the effect of the coupling slot and side cavity. Therefore, the calculated values of ZT^2 must be adjusted downward. Based on Los Alamos experience[11] we expect ZT^2 to be 12.5% lower for the complete SC structure. Work done with the MAFIA[12] three dimensional field codes provides a rough confirmation of this estimate. Additionally, some small adjustment should be made to account for surface imperfections and brazing artifacts. We assume a further 2% reduction of the SUPERFISH values for ZT^2 for these effects. In Figure 8 the quantities ZT^2 and T are plotted as functions of β from adjusted SUPERFISH results. In Figure 9 the maximum surface gradient is plotted, normalized to an average axial gradient of E_o=1 MV/m. For this optimization of the SCS, the average effective accelerating gradient when the cavities are excited to a given E_{max} rises slightly with increasing β while the power dissipation per meter drops significantly.

The smooth curves in Figures 8 and 9 are third order fits to the SUPERFISH results. These fits are employed to calculate the length and number of cells needed to reach the design energy subject to the constraints on peak field and power dissipation.

c. Segmentation of the Structure

The division of the Linac into seven independently excited rf modules results from three principal considerations, namely the practical size for 800 MHz klystrons, the shunt impedance of the structure, and the existence of suitable penetrations from the equipment gallery into the linac vault for the waveguides. Uniform distribution of the rf power favors feeding the modules from the center, so there is a coupler at that location which can accommodate a quad also. Rf defocusing requires that the quads of a FODO channel be less than two meters apart in the first modules. Symmetry with respect to the rf feed point requires an even number of sections per module. The modules must be divided into four sections to keep the transverse beam size within the selected beampipe aperture.

The required number of accelerating gaps and the manner of dividing them up between modules is determined iteratively from the structure calculation. The ratio of the maximum surface field E_{max} to the average axial field E_o is known as a function of β from the

SUPERFISH results. The number of accelerating gaps required to raise the energy from 116 MeV to 400 MeV is calculated subject to the condition E_{max} = 44 MV/m in every cell from $E_o(\beta)$, $T(\beta)$, and $Z_{sh}(\beta)$ as represented by the third order fits. The cells are then divided into seven groups of equal dissipation including loading from a 50 mA beam current. Each of the seven modules are subdivided into four sections with the same number of cells. The acceleration is then recalculated iteratively to determine a constant cell length $\bar{\beta}\lambda/2$ for each section where $\bar{\beta}$ is the β corresponding to the average energy in the section for a particle that enters and leaves the section with the correct phase ϕ_s. The parameters for each section of the linac are given in Table 3.

d. Transverse Focusing

The rf power distribution scheme results in a symmetric arrangement of accelerating sections with a coupler at the midpoint. The further segmentation required to provide for transverse focusing can be established by calculation of the growth of the beam envelope from a waist in the structure to a proposed quad location. The rf defocusing has its greatest strength relative to the focusing quads at the low energy end of the linac where the unnormalized transverse emittance is also highest. Furthermore, there is more transverse tune spread arising from the bunch width of $\pm$20 degrees at injection into the first accelerating section of the 805 MHz structure. The overall character of the focusing scheme follows from the appropriate distance between elements established for the first module, the lattice type selected, and the sequence of module lengths resulting from the requirement for the same rf power per module.

Module /Sect.	E_i [MeV]	ΔE [MeV]	L_{rf} [m]	L_{sep} [m]	$\bar{\beta}$	P_{Cu} [MW]	P_{beam} [MW]	S_{quad} [kG]	Ph. Adv. [deg] H	V	L
1											
1	116.54	8.11	1.293	0.262	0.4632	1.72	0.41	17.44			
2	124.65	8.33	1.329	0.269	0.4760	1.74	0.42	-17.74	69	62	107
3	132.98	8.55	1.364	0.276	0.4886	1.75	0.43	17.81			
4	141.53	8.76	1.398	0.500	0.5008	1.66	0.44	-16.81	68	66	108
		33.74	5.384	1.307		6.87	1.69				
			6.691			8.56					
2											
1	150.30	8.88	1.432	0.290	0.5127	1.76	0.44	17.34			
2	159.18	9.08	1.464	0.296	0.5242	1.77	0.45	-17.15	66	60	105
3	168.25	9.23	1.495	0.302	0.5355	1.79	0.46	17.32			
4	177.52	9.45	1.526	0.500	0.5464	1.69	0.47	-16.40	64	61	102
		36.67	5.917	1.388		7.01	1.83				
			7.305			8.84					
3											
1	186.97	9.53	1.556	0.314	0.5571	1.80	0.48	16.95			
2	1.9650	9.70	1.585	0.320	0.5674	1.81	0.48	-16.49	64	55	100
3	206.21	9.87	1.613	0.325	0.5774	1.83	0.49	17.01			
4	216.08	10.03	1.640	0.500	0.5872	1.73	0.50	-16.13	62	56	97
		39.14	6.394	1.459		7.17	1.96				
			7.853			9.13					
4											
1	226.10	10.08	1.667	0.336	0.5967	1.83	0.50	16.56			
2	236.19	10.23	1.692	0.341	0.6058	1.84	0.51	-15.88	61	52	96
3	246.42	10.37	1.717	0.346	0.6148	1.87	0.52	16.60			
4	256.79	10.51	1.742	0.500	0.6235	1.76	0.53	-15.93	59	53	93
		41.19	6.818	1.523		7.30	2.06				
			8.341			9.36					
5											
1	267.30	10.54	1.765	0.355	0.6319	1.86	0.53	16.24			
2	277.83	10.66	1.788	0.360	0.6401	1.88	0.53	-15.35	58	48	91
3	288.50	10.79	1.810	0.364	0.6480	1.89	0.54	16.09			
4	299.28	10.91	1.832	0.500	0.6558	1.79	0.55	-15.60	56	50	81
		42.89	7.195	1.579		7.42	2.14				
			8.744			9.56					
6											
1	310.19	10.91	1.853	0.373	0.6632	1.89	0.55	16.00			
2	321.10	11.02	1.873	0.377	0.6705	1.91	0.55	-15.03	54	45	86
3	332.12	11.13	1.893	0.380	0.6776	1.92	0.56	15.67			
4	343.25	11.23	1.912	0.500	0.6844	1.81	0.56	-15.06	53	47	86
		44.30	7.531	1.630		7.53	2.22				
			9.161			9.74					
7											
1	354.48	11.22	1.930	0.388	0.6911	1.91	0.56	15.47			
2	365.70	11.31	1.948	0.391	0.6975	1.92	0.57	-14.81	51	43	84
3	377.02	11.41	1.966	0.395	0.7038	1.93	0.57	15.51			
4	388.42	11.50	1.983	0.000	0.7099	1.83	0.58	-15.15	50	44	82
		45.44	7.827	1.174		7.59	2.27				
			9.001			9.86					
Final	399.92	283.38	47.066	10.060		50.89	16.15				
			57.126			67.04					

Table 3: Parameters of the 400-MeV linac listed for each accelerating section

For each choice of quad spacing there is a particular β_{min}, the width Twiss parameter at the waist, for which the beta function at the quad β_{max} has it minimum value. The values β_{min} and β_{max} can be used as fitting conditions at the beam waists along the structure to determine the required quad strengths. Because the optimum power distribution for the optimized SC structure leads to a fixed number of cells per section, the section lengths increase smoothly with energy, and the same β_{min}, β_{max} pair can be used for all focusing cells. Because the low energy modules are shorter, four sections per module are sufficient to get the required quad spacing at low energy. Figure 10 shows the initial beam ellipses, final beam ellipses and the beam envelopes along the linac in all the planes on the basis of the parameters in Table 2. This figure and the quad strengths to match the β_{min}, β_{max} values were calculated by the program TRACE 3-D which takes account of rf defocusing and space charge in a linear approximation.[13] Particle dynamics calculations have been made which verify the TRACE 3-D results. Some results of the dynamics calculation for the linac and transition section are presented in Section III.C where the transition section is described. Table 3 includes the quad strengths and phase advance of the transverse oscillations.

The possibility of using quad doublets or triplets instead of the FODO scheme has been examined. Because couplers dissipate some rf power and take up scarce space, it is appealing to reduce the number of couplers by focusing in both planes at each break in the accelerating structure. However, the beam spreads too fast to be contained by multiplets only between modules. Therefore, the center coupler must contain a multiplet. For a doublet the coupler is $3\beta\lambda/2$ long, and for a triplet it must be $5\beta\lambda/2$. Much stronger quads are needed in closely spaced multiplets than in FODO cells. If electromagnetic quads are to be used in the couplers, additional problems of cooling and magnet design are raised. The stigmatic focusing of doublets plus the more critical setting and alignment tolerances complicate routine tuning considerably. However, the beam will usually be guided through a FODO channel even if the gradients are set crudely. The tuning and matching properties of a symmetric triplet scheme seem more tidy, but settings are critical. The length devoted to focusing components, tuning critically and high gradients required argue against it. These and similar options will be

evaluated further as part of the detailed design process; they have only minor relevance to the parameters specified in Tables 2 and 3.

The first steps of the electrical design of an electromagnetic quadrupole have been carried out. The aim has been to proceed sufficiently far to establish the field quality, electrical parameters, and approximate mechanical properties. Figure 11 shows the conceptual design for a cross-section of an octant. The coil window is filled by two twelve-turn coils for each pole, excited in parallel. It has been sized to contain enough copper that no direct cooling of the coil should be required for pulsed operation at maximum design gradient. The poles are excited with a parallel current feed to reduce the inductance. Calculated magnetic field properties and estimated electrical properties are given in Table 4. The saturation curve used is the default in the POISON program; eddy current effects have not been calculated. The magnetic length has been set at 8 cm to establish the possibility of using such a quad in shorter, $\beta\lambda/2$ couplers. It is also advantageous to save space between modules however, to prevent debunching. Therefore, if the current choice of $3\beta\lambda/2$ remains the preferred one, the quadrupoles will not be lengthened to fill them.

Aperture radius (r_p)	0.02	m
Magnetic length (l_{eff})	0.08	m
Maximum required gradient (B'_{max})	264.	kG/m
Number of turns per pole	12	
Current for B_{max} (I_{max})	350.	A
Resistance (R)	2.1	mΩ
Inductance, parallel connection (L)	32.9	μH
Pulse length	~1.	ms
Peak voltage (V_{max})	~150.	V
Duty factor	1.5	%
Peak real power (P)	812.	W
Average power (P)	12.	W
Gradient error at 1.5 cm	<1.	%

Table 4: Properties of an Electromagnetic Quadrupole

B. RF and Power Modulation System

The reference design for the 805 MHz Linac Upgrade requires seven high power klystron and modulator sections to increase the output energy of the Linac to 400 MeV. The specifications for the klystron and modulator are shown in Table 5 and Table 6.

Peak power output	12 MW
Pulse length	125 μs
Pulse repetition rate (PRR)	15 pps
Duty factor	0.1875%
Average power	22.5 KW
Efficiency	50%
Gain	50 db
Rf output	WR975 waveguide
Dimensions	108 inch height 24 inch dia.
Voltage	200 KV
Current	120 A

Table 5: Klystron Specifications

Voltage	210 KV
Voltage regulation	±0.5%
Current	125 A
Pulse length	125 μs
PRR	15 pps
Peak power	26.25 MW
Average power	45 KW
Pulse flatness	±0.5%
Rise time	2 μs
D.C. power supply	20 KV at 2.5 A
Dimensions (W x L x H)	6ft. x 16ft. x 10ft.

Table 6: Modulator Specifications

The schematic block diagram for a typical rf station is shown in Fig. 12. The system contains rf feedback loops referenced to the output of the klystron via directional couplers and to the SCS module via pick-up loops to regulate the rf amplitude to ±0.2% and phase to ±1 degree.

The system can be divided into four sections:

1. The low level rf (LLRF) consisting of the master oscillator, programmable fast phase shifter and attenuator, feedback amplifiers, directional couplers and pickups.

2. Driver amplifier, 100 W.

3. High level rf (HLRF), 12 MW klystron.

4. DC power module consisting of D.C. power supply, pulse forming network (PFN) and modulator, PFN voltage regulator and step-up pulse transformer.

A exploded pictorial assembly of the D.C. power module is shown in Fig. 13 without the D.C. power supply. The D.C. power supply can be located away from the module if desired. Figure 14 and 15 show schematic and pictorial views of the regulator circuit and modulator circuit, respectively. Fig. 16 shows a pictorial view of the klystron and pulse transformer.

C. Transition Section

The increase in rf frequency, from 201.25 to 805 MHz for the side-coupled cavity following tank 5 of the drift tube linac, will rescale the particle bunch length in energy-phase space proportionally. Because the bucket restoring forces in the 805 MHz structure are stronger than those of the previous drift tube structure, a mismatch will occur between the beam bunch size and its enclosing accelerating bucket, whose average accelerating gradient (7.5 MeV) is needed to achieve the 400 MeV output energy. To prevent the beam bunch from tumbling severely in the longitudinal plane as a result of this new dynamic environment, a special matching section will be replaced between the drift tube linac and the side coupled accelerating structure, to provide a smooth transition of the particle bunch forces.

Kinetic energy (T)	116.54	MeV
ϵ_L (90%, invariant)	6.2×10^{-5}	πeVs
ϵ_T (90%, unnormalized)	10.	πmm-mrad
Twiss parameters		
β_x	2.49	m
α_x	0.	
β_y	5.25	m
α_y	-0.41	
β_ϕ	0.068	deg/keV
α_ϕ	0.30	deg/keV/m
Beam current, averaged over pulse (I_b)	50.	mA
Tank 5 frequency (f)	201.25	MHz
Effective tank 5 gradient (E_oT)	1.82	MV/m
Tank 5 accelerating phase (ϕ_s)	-32.	deg

Table 7: Beam characteristics at the 116 MeV point in the present Fermilab Linac (end of tank 5)

Table 7 collects important properties of the 116-MeV H^- beam leaving tank 5 of the 201.25 MHz Alvarez linac. The entries are based on a combination of measurements at 10 MeV and PARAMILA simulations, using the best available information on tanks 2-5. Unfortunately there is insufficient space in the existing linac structure to measure beam properties at 116 MeV. Therefore the design of the transition section must provide a range of operating parameters sufficient to accommodate the expected variations in the 116-MeV beam properties.

The transition module must also provide for transverse matching and the current uncertainty in the Twiss beta of the incoming beam (typically 5%). Although one could to some degree adjust the Alvarez tank 5 beam to the new 805 MHz structure, a finely matched beam provided by this extra non-accelerating structure is important in providing low emittance growth for the overall 400-MeV system. It will be seen that provision for this precise matching does not significantly complicate the design; therefore tank 5 can be setup for optimum performance without regard for requirements of the new structure. The more important numbers in Table 7 are the energy, emittances and beam intensity. The calculated beam ellipses are used for specificity, and are at the extreme of expected beam behavior, to provide assurance of design flexibility for a wide range of operating conditions.

The last cell in the Alvarez tank 5 is 67 cm long, while the first focusing interval (transversely) in the new linac is 153 cm (F to D). To provide smooth beta matching transversely, one would normally design the transition section to have a length equal to the geometric mean of 67 and 153 cm. Such a choice, when applied to the longitudinal plane, implies a length and gradient in the non-accelerating structure that correspond to a quarter synchrotron wavelength, and the geometric mean of the z-plane focusing force. For the present design we match using an 805 MHz structure. This corresponds to 60 rf cells operating as bunchers with an effective acceleration gradients (E_oT) of 0.5 to 0.8 MeV/m, depending on the input z-plane ellipse orientation. A special low rf power, 805 MHz power supply will be provided for the transition section.

The precise values for the longitudinal match are expected to require tuning from variation in operating conditions. Therefore a minimum two degrees of freedom is achieved by dividing the power feed into two independently adjustable parts. Beam ellipses and beam envelopes for the transition section are shown in Figure 17. The corresponding parameters are collected in Table 8.

Section	E_oT (MV/m)	l_{rf} (m)	l_{sep} (m)	S_Q (kG)
			0.168	-8.84
1	0.710	1.277		
			0.255	12.90
2	0.710	1.277		
			0.255	-17.75
3	0.558	1.277		
			0.255	13.46
4	0.558	1.277		
			0.500	-16.93
		5.106	1.433	
		6.539		

Table 8: Transition section parameters

The transverse matching has been chosen with a quadrupole interval of 153 cm corresponding to four rf sections of 15 cells each. This provides the sufficient degrees of freedom to match all Twiss parameters in both transverse planes. Because the rf gradients are so low here, one can provide larger quad and rf structure bores to accommodate the irregular transverse beam dimensions, with negligible power penalties. An alternative option of six rf sections of 10 cells, would provide additional tuning flexibility, and less disruptive transverse beam envelopes, but with a penalty of extra bridging sections.

To test the effectiveness of this transition section, numerical simulations were performed using the codes PARMILA and DDYNZ to track the linac beam through tanks 2-5, the transition section and the final seven side-coupled modules. The SCS parameters from Table 3 were used in this simulation. The results are shown in Figures 18-21. Figure 18 shows the rms bunch z-radius expressed in rf degrees along the length of the 805 MHz structure. The effect of the transition section in reducing the bunch z-dimension is shown.

Residual damped synchrotron oscillations are evident. These oscillations are created by the large drift regions between sections that provide space for beam diagnostics. Figure 19 shows the variation of longitudinal emittance along the new linac. No evidence of z-plane dilution is seen at the design current of 50 mA.

Figures 20 and 21 show the x-plane beam radius, for a 90% beam envelope, through the transition section and the 28-section acceleration system. The radial excursions in the transition section are seen not to be severe. The quadrupole tune regions simulated were all less than 60 degree phase advance including the space charge depression (typically 10% for a 50 mA design beam). Predicted transverse emittance growth was typically 10% to 20% for the 90% beam envelopes at the 50 mA design current.

D. Linac Beam Diagnostics

Presently the 200-MeV emittance is measured by obtaining profiles on three wires in a drift space going to the straight-ahead dump from the Linac (Figure 22). Two quadrupoles before the wires focus the beam to produce a waist near the center wire for improved emittance resolution. No change in this procedure or equipment would be necessary for the 400-MeV beam.

The momentum of the 400-MeV H^- Linac beam could not be measured by the present spectrometer magnet. At a field of 16.7 kG necessary for 400 MeV essentially all of the H^- beam would be stripped in the first five centimeters. With the present magnet at 200 MeV (B=11.265 kG, L=1.33 meters), 0.2% of the beam is stripped going through the magnet. To keep the stripping for a 400-MeV beam to the same level (0.2%) the field would have to be reduced to 7.5 kG and the path length increased to 3 meters to retain the 40 degree bend. Such a magnet would be large, expensive, difficult to install and require a significant change in the transport optics that maybe unattainable in the space required.

Use of the 40 degree momentum dump is desirable for continuous dumping of the Linac beam. The momentum dump was constructed with a larger steel casting and has an estimated dissipation of 3 to 10 kW while the straight-ahead dump has a dissipation in the range of 0.3 to 1 kW. Typical linac pulses at 400 MeV and 15 pulses per second

produce 7.2 kW, requiring the momentum dump. With pulses of once per second or less either dump is usable, but the momentum dump would still be preferred.

Our proposal is to place a thin foil in the H^- beam to strip to protons. By stripping the H^- beam before the present spectrometer, the momentum dump can still be used, allowing relative momentum and momentum spread measurements. Foils of 200 $\mu gm/cm^2$, as used at the booster injection, strip both electrons at 98% efficiency or better with an energy loss to the proton of less than 1 keV at 200 MeV. At 400 MeV the stripping cross section is reduced by a factor of 1.5 so the foil thickness should be increased to 300 $\mu gm/cm^2$ to give the same stripping efficiency. To accommodate 400-MeV protons requires increasing the power supply current from 100A to 150-200A to obtain 16.7 kG in the spectrometer. Operating the spectrometer at this level should be possible, but it must be tested for cooling, saturation and field uniformity.

E. Transfer Line to Booster

The present 200-MeV transfer line (Fig. 23) from the Linac to the Booster contains an electrostatic chopper and a magnetic septum to remove a portion of the linac beam and deflect it into the Booster line, four major bends (two vertical bends to get from the Linac to the Booster level) and 26 quadrupoles for matching and achromatic correction. Several multi-wire profile monitors and beam current toroids provide monitoring while horizontal and vertical trim steering magnets allow small corrections. Assuming that the basic design of the present line will be retained for the 400-MeV Upgrade, operation with an H^- beam will require replacement of several major elements.

At 400 MeV the momentum is approximately 50% larger than at 200 MeV (954 vs. 644 MeV/c), requiring that the fields in the bending magnets MH1, MV1 and MV2 be increased to over 6 kG (Table 9). At this field and path length, stripping of the H^- ion will be less than 0.1%. However in MH2 the field will be 12.3 kG causing considerable stripping and a loss of the beam. Replacement of MH2 with a magnet of 50% to 70% greater length will be required.

Bending Magnet	Angle (deg)	Length (m)	Field (kG) 200 MeV	400 MeV	Field (kG) at 400 MeV for Stripping<0.1%
MH1	5.925	.495	4.49	6.65	7.9
MV1	-12.83	1.16	4.14	6.13	7.6
MV2	12.83	1.16	4.14	6.13	7.6
MH2	-24.62	1.11	8.31	12.3	7.6

Table 9: Bending Magnet Parameters

Quadrupoles in the line are capable of running at 55A without heating problems. Operation at 400 MeV would cause some quads (six or seven) to exceed this limit and would require replacement if retuning or repositioning is not possible. At 50 A the pole-tip field is less than 4 kG so stripping is negligible.

The plates of the electrostatic chopper are 143 cm long, separated by 2.54 cm, and operate at 60 kV. Reducing the separation or increasing the voltage is impractical because of electrical breakdown, so replacement with a longer chopper is necessary. The septum is 104 cm long and operates at a field of 3.2 kG (125, 9900 A, pulsed). Operation at 400 MeV will require 4.8 kG, a possibility that needs to be considered for heating and saturation; otherwise replacement will be necessary.

Since the chopper immediately follows the last linac cavity, focusing for a narrow horizontal beam at the septum is presently achieved using the quadrupoles within the last four drift tubes of the Linac. Removal of the drift-tube linac and replacement with a side-coupled linac which has quadrupoles only between cavities will require some space between the new linac structure and the chopper to allow for two or three quadrupoles to give sufficient focusing.

Many of the power supplies should be usable in 400-MeV operation. Unless a higher voltage is chosen for the chopper this supply is still useful. The quadrupoles currently have supplies that allow for 50A operation and except for quadrupoles that are replaced, no change in the supply is necessary. The septum will require a new supply as will some of the bending magnets.

F. Debuncher for Booster Injection

The longitudinal phase space area of the Booster beam is proportional to the energy spread of the Linac bunches. This is because all Linac bunches are "debunched" during the first 30 revolutions or so, and the resulting unbunched beam is captured into the usual 84 bunches by the Booster rf. This debunching process is not adiabatic since the phase space area of the final unbunched beam is not the sum of the areas of the individual Linac bunches. Consequently a debuncher which reduces the energy spread by rotating the phase space ellipse of each Linac bunch is essential to reduce the longitudinal phase space area of the resulting Booster beam.

The present 201.25 MHz debuncher is located approximately 40m from the end of the Linac, a distance which is less than optimal for this frequency and phase space area (.15 MeV-nsec). A better location for an 805 MHz debuncher is between Q12 and MV2 (see Fig. 23), approximately 27m from the end of the 805 MHz accelerating structure. Bunches of .15 MeV-nsec phase space area drift to a phase width of about ±60 degrees, where a four-cell cavity ($2\beta\lambda$) at 4.3 MeV/m reduces the energy spread to less than 0.5 MeV, as shown by numerical simulations in Fig. 24.

Figure 24a shows a matched ellipse at 400 MeV emerging from the Linac. After drifting 27 m, the ellipse has drifted to appear as in Fig. 24b. Application of 4.3 MeV/m by the four $\beta\lambda/2$ cells will rotate this ellipse to appear as in Fig. 24c. In these figures, the horizontal line extends ±60 degrees, and the vertical marks are at ±1 MeV. These results are very promising, but to pursue this further, it will be necessary to take into account, (1) space charge in the beam and (2) effects of dispersion and path length differences in the beam transport line from the Linac and the debuncher.

G. Injection into Booster

Like the transfer line, the present H^- charge-exchange injection system, located in the first of 24 6-meter long straight sections in the Booster, requires no fundamental design changes, but scaling the design to the new momentum necessitates replacement of some components. This is fortunate in a way: the present injection

apparatus is quite complicated because it was required to accommodate the previously used single-turn and multiturn proton injection methods as well as the current standard H^- injection method, and replacement of components can be accompanied by considerable simplification of the system.

Figure 25 shows the layout of the present H^- injection system. (Components formerly used for proton injection are not shown.) A current-sheet septum magnet deflects the incoming beam onto a path parallel to the closed orbit. The beam then encounters the first of two so-called orbit-bump magnets (orbumps) which are each back-to-back single-turn pulsed dipoles. The orbit-bump magnets displace the closed orbit parallel to its normal path onto the stripping foil during the injection process and displace the incoming negative beam onto the same orbit, whereupon it merges with previously injected circulating beam after stripping by the foil. When injection is complete, the orbit bump decays, moving the circulating beam off the foil in about 30 microseconds.

The current-sheet septum magnet is similar to the one downstream of the chopper and the same situation applies: raising the strength 47% puts both the magnet and its power supply close to their design limits, and testing is necessary to determine whether they will run gracefully at the higher excitation.

Since the beam size adiabatically shrinks from 200 to 400 MeV, the stripping foil can be located about 21% closer to the centroid of the circulating beam than it is now while maintaining the same safety factor. Hence the present orbit-bump magnets need not be 47% stronger but only about 21%. However, even this smaller increase probably exceeds the capabilities of the magnets and power supply. A reasonable solution is to replace the magnets with new ones which are about 10% longer but have the same field strength and somewhat smaller horizontal aperture. The required increase in length is 10% rather than 21% because the displacement at the foil scales as the square of the length (one power for the added integrated strength and one power for the added lever arm). With these changes, the required current will be the same and the inductance, and hence the required voltage, will also be about the same as at present; thus the present power supply, which is an expensive one, can be reused. The space

required to accommodate the added length can be obtained by reducing the length of the foil-changer and/or by moving the septum magnet upstream.

The effects of the stripping foil on the beam depend on the energy. The relevant stripping cross sections decrease by about a factor of 1.5 from 200 to 400 MeV. The present standard carbon foil of 200 $\mu gm/cm^2$ surface density converts H^- to H^+ with an efficiency of about 99%. A thickness of 300 $\mu gm/cm^2$ would then give about the same conversion efficiency at 400 MeV.

The multiple scattering of a 200-MeV beam in a 200 $\mu gm/cm^2$ foil increases the normalized 95% emittances by about 3π mm-mrad vertically and by about 1π horizontally for the average number of passes during the injection process. The emittance growth for a given duration of injection scales linearly with the thickness and inversely with momentum and velocity. So the emittance growth for a 300 $\mu gm/cm^2$ foil at 400 MeV would be about 18% smaller than for 200 $\mu gm/cm^2$ at 200 MeV.

H. Building Modifications

The new higher-gradient cavities will be installed on the gallery side of the linac enclosure (Figs. 26, 27, and 28). Unused penetrations in the shield wall between the enclosure and the gallery basement already exist so that the 805 MHz rf waveguide conveying the drive power to the new modules can be routed directly to the modules without making major building modifications. The length of the seven new modules and transition section will be the same total length as the drift-tube tanks that they replace.

The new klystron power supplies will be installed in the gallery space adjacent to the existing power supplies. To create sufficient space, existing office areas will be converted and the building will be enlarged. The present wall and precast fascia will be removed and new roof structure installed. Figures 27 and 28 show the components of the seven new klystron power supplies installed in the enlarged Linac Gallery.

The two-story building addition adjacent to the Linac Gallery will provide areas for the new klystron power supplies, technician

work space, office space, system staging, mechanical equipment and toilet space. Partitions are used only around power supplies, toilets and mechanical equipment. Open planning is used for the office and tech work spaces similar to many other existing areas at Fermilab. Building modifications will be designed according to DOE Order 6430.1.

Additional utilities will be required to operate the new systems. Two new 1.5 MVA substations with a new high voltage feeder and switch will supply power for both the new systems as well as for the new office/tech work space. Additional capacity will be provided for the existing Linac low conductivity water (LCW) cooling systems. Fire detection and suppression systems for both equipment systems and building space will be provided. Ventilation of the new power supply equipment and HVAC for new building space are included.

The construction of the new building space will be done so as to minimize impact on the operating schedule of the present 200-MeV linac. Very substantial temporary barriers, dust partitions and roof covering will be installed at the onset of the job. Special precautions with approved techniques will be used for the removal of existing asbestos insulation on concrete fascia panels that are to be removed. Heavy shoring under existing precast panels and roof trusses will be installed so that removal and demolition may be accomplished with minimum disruption to operations. Electrical and cooling system additions will be installed and tested and connected on line with minimal outages.

The installation of the new high gradient cavities and power supplies will be done with minor disruption in the operating schedule of the present 200-MeV linac. The new modules can be installed in the linac enclosure during short maintenance and development periods without disturbing the operating systems. The klystron power supplies will be installed and operated in the new space made available by the building modifications already described. The modules can be conditioned and run at full power independent of the operation of the drift-tube cavities. When all components have been fabricated and tested a change-over time of several month duration will be scheduled. During that time, the old linac tanks are moved laterally in the enclosure and the new modules are moved onto the beamline (see Fig. 29). At the same time, the modifications are made

to the beam diagnostics area and the transport and injection system to the Booster accelerator. The systems are then commissioned at the higher energy of approximately 400 MeV.

References

1. L.J. Laslett, in BNL-7534, pg. 324. (1963).

2. L.M. Young and J.M. Potter, "CW Side-Coupled Linac for the Los Alamos/NBS Racetrack Microtron", IEEE Trans. Nuc. Sci., Vol NS-30, No. 4, pg. 3508 (1983)

3. V.D. Burlakov, et al, "Status of the Construction of the INR Meson Factory", Proc. of the 1984 Linear Accelerator Conference, GSI, Darmstadt, GSI-84-11, pg. 9-13 (1984).

4. V.K. Grishin, et al, "Computer Simulation of the RF Properties and Thermal Conditions of the Disk-and-Washer Accelerating Structure for the Racetrack Microtron", Nuc. Inst. and Methods in Phys. Res. A255, pgs 431-436 (1987).

5. S. Inagaki, "Disk-and-Washer Cavities for an Accelerator", Nuc. Inst. and Methods in Phys. Res. A251 (1986) pgs. 47-436.

6. R.J. Noble, "Acceleration Gradient for the 400-MeV Linac Upgrade", Fermilab TM-1448 (1987).

7. W.D. Kilpatrick, "Criterion for Vacuum Sparking Designed to Include Both RF and DC", Rev. Sci. Inst. 28, 824 (1957).

8. S.O. Schriber, "Factors Limiting the Operation of Structures under High Gradient", Proc. of the 1986 Linear Accel. Conf., Stanford, CA, p. 591.

9. R. Lehmann, "Experiments with an RFQ Sparker", Particle Accel. 22, 161 (1987).

10. C.W. Owen, C.A. Radner and D.E. Young, "High Field Measurements at 200 MHz in Conventional Linear Accelerator Geometries at 5,50, and 130 MeV", Proc. of the 1966 Linear Accel. Conf., LANL-8, 3609, Pgs. 176-182 (1966).

11. L.M. Young, LANL, private communication.

12. M.J. Browman, R. Cooper, and T. Weiland, "Three-Dimensional Cavity Calculations", Proc. of the 1986 Linear Accel. Conf., SLAC, 1986.

13. K.R. Crandall, "TRACE 3-D Documentation", LANL report LA-11054-MS (August, 1987).

Appendix A

Antiproton-Proton Collider Upgrade - Linac Schedule

APPENDIX A

TEVATRON UPGRADE - LINAC SCHEDULE

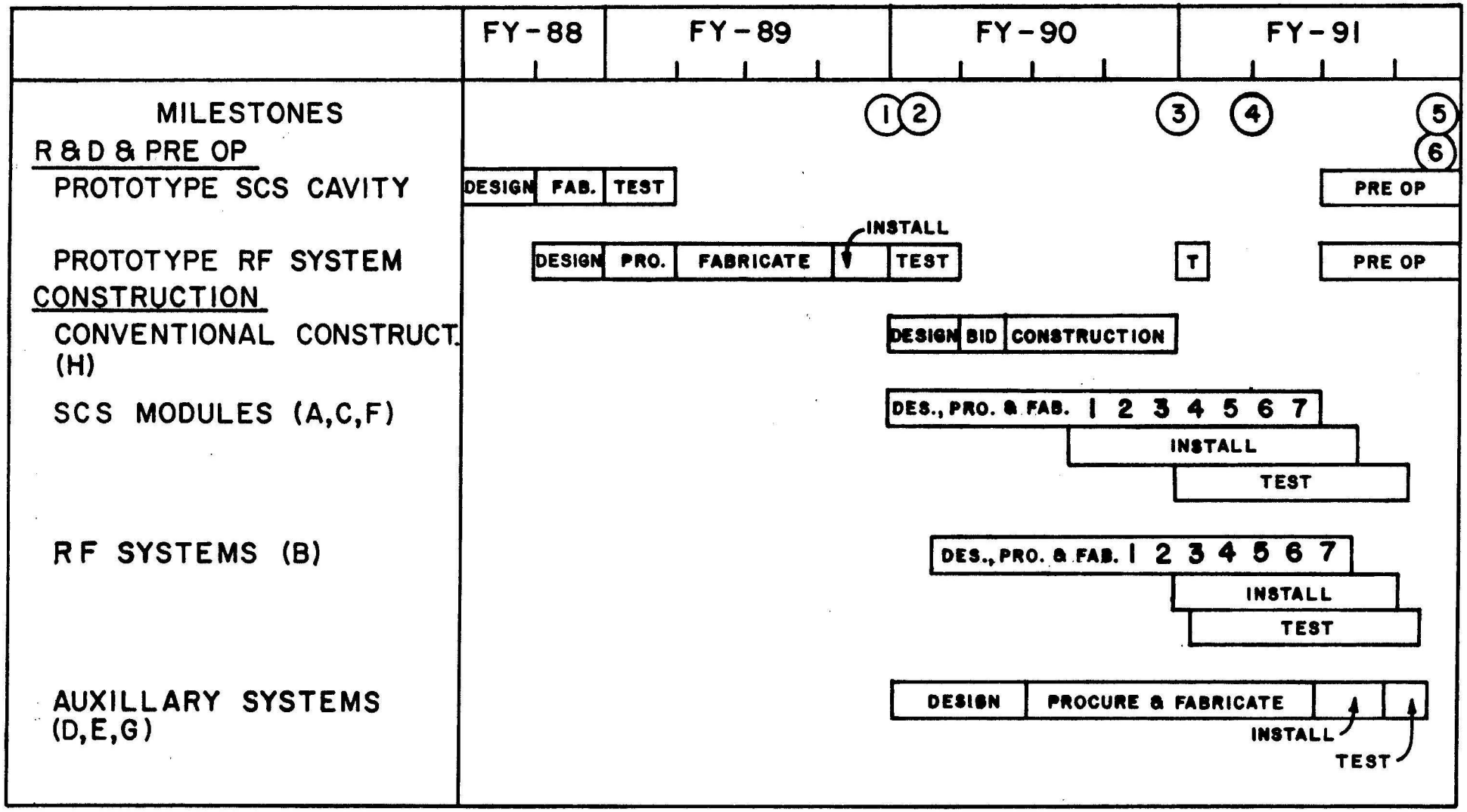

No.	Milestone	Date
1	Start Project	October 1, 1989
2	Specify RF System	November 15, 1989
3	B.O. Of Power Supply Gallery	September 30, 1990
4	Full Power Test of 1st Module	January 1, 1991
5	Conversion to 400-MeV Injector	September 30, 1991
6	Complete Project	September 30, 1991

Appendix B

Antiproton-Proton Collider Upgrade - Linac Cost Estimate

Antiproton-Proton Collider Upgrade -Linac Cost Estimate
(FY-1988 K$)

A.	SCS Accelerator Cavity Systems		5,310
	A.1	Accelerating cavities including brazing (28 sections)	3,470
	A.2	Tuning lab	230
	A.3	RF feed cells (21 units)	200
	A.4	Quadrupoles w/P.S. (32)	170
	A.5	Beam diagnostics	320
	A.6	Stands	190
	A.7	Cooling system	140
	A.8	Vacuum	340
	A.9	Installation	250
B.	RF Power Supply Systems		5,140
	B.1	Power supply and filters (8 units)	560
	B.2	Pulse forming networks (8 units)	1,250
	B.3	Klystron w/solenoid, oil tank, transformer (8 units)	2,265
	B.4	Transmission waveguide	535
	B.5	Controls and interlocks	320
	B.6	Dummy load and test equipment	50
	B.7	Installation	160
C.	Transition Section		880
	C.1	RF cavities including brazing (4 sections, 52 cells)	385
	C.2	Tuning lab	20
	C.3	RF power supply	300
	C.4	RF feed cells	20
	C.5	Quadrupoles w/PS (6)	30
	C.6	Beam diagnostics	30
	C.7	Stands	20
	C.8	Cooling system	15
	C.9	Vacuum	30
	C.10	Installation	30

D.	Linac 400-MeV Beam Diagnostics	110
	D.1 Stripping equipment	20
	D.2 Beam position, profile, and intensity monitors	40
	D.3 Powers supply replacement	50
E.	Booster Transfer Line	380
	E.1 Replace MH-2	30
	E.2 Chopper	15
	E.3 Septum replacement	20
	E.4 Quadrupole coil replacement	50
	E.5 New steering elements w/PS (10 units)	50
	E.6 New power supplies	140
	E.7 Diagnostics and controls	35
	E.8 Installation	40
F.	Debuncher for Booster Injection	570
	F.1 Cavities, supports, vacuum (4 cells)	210
	F.2 RF power supply	320
	F.3 Controls	30
	F.4 Installation	10
G.	Injection into Booster	230
	G.1 Stripper	10
	G.2 Septum	20
	G.3 New orbumps	50
	G.4 Septum power supply	40
	G.5 Mechanical, vacuum, water	40
	G.6 Installation	70

H.	Building Modifications	1,630
H.1	Sitework, earth work, paving	120
H.2	Demolition and protection	160
H.3	Concrete foundations	150
H.4	Structural and misc steel	190
H.5	Precast concrete walls, panels and blocks	130
H.6	Roof closures, partitions, windows and doors	140
H.7	HVAC and process piping	200
H.8	Cooling system rf power supplies	60
H.9	Electrical substation (13.8 Kv)	90
H.10	Electrical distribution	190
H.11	Fire Protection and plumbing	200
Total Construction Costs		14,250
Engineering, Design, Inspection and Administration(1) (16% of M&S)		2,280
		16,530
Contingency (20% of above costs)		3,300
		19,830
Incremental Overhead(2)		140
		19,970
Escalation:		
(i)	Conventional construction to mid 1990(3)	150
(ii)	Special facilities to 1st qt. 1991(3)	1,880
Total Estimated Cost in Then-Year K$		22,000

(1) Administration costs include Fermilab project management costs.

(2) Included in this category are the incremental support from the Fermilab Business and Services Section and for the purpose of the cost estimate is taken as 0.7%.

(3) Using DOE escalation rates.

Figures

Figure 1

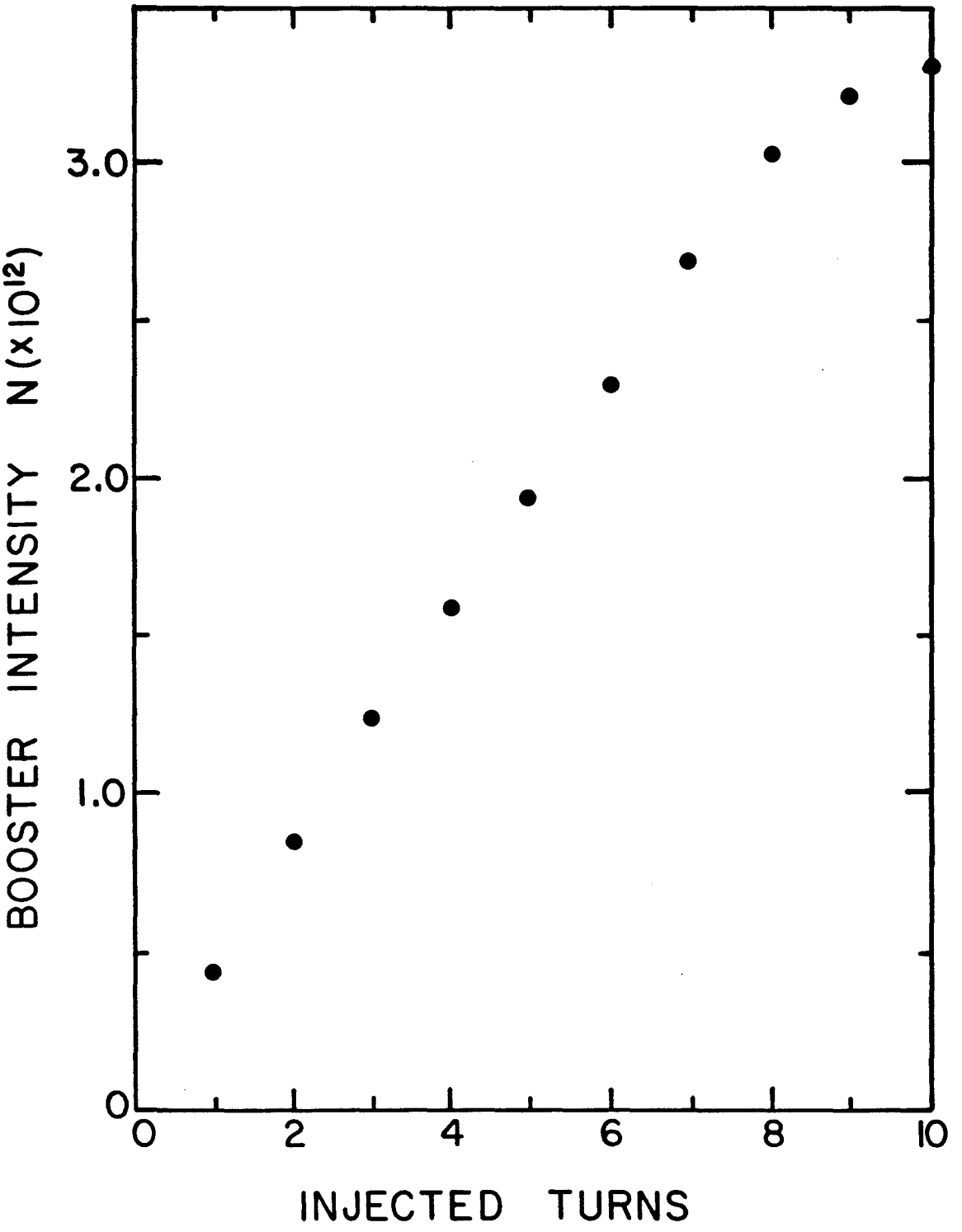

BOOSTER INTENSITY VS. NUMBER OF INJECTED TURNS

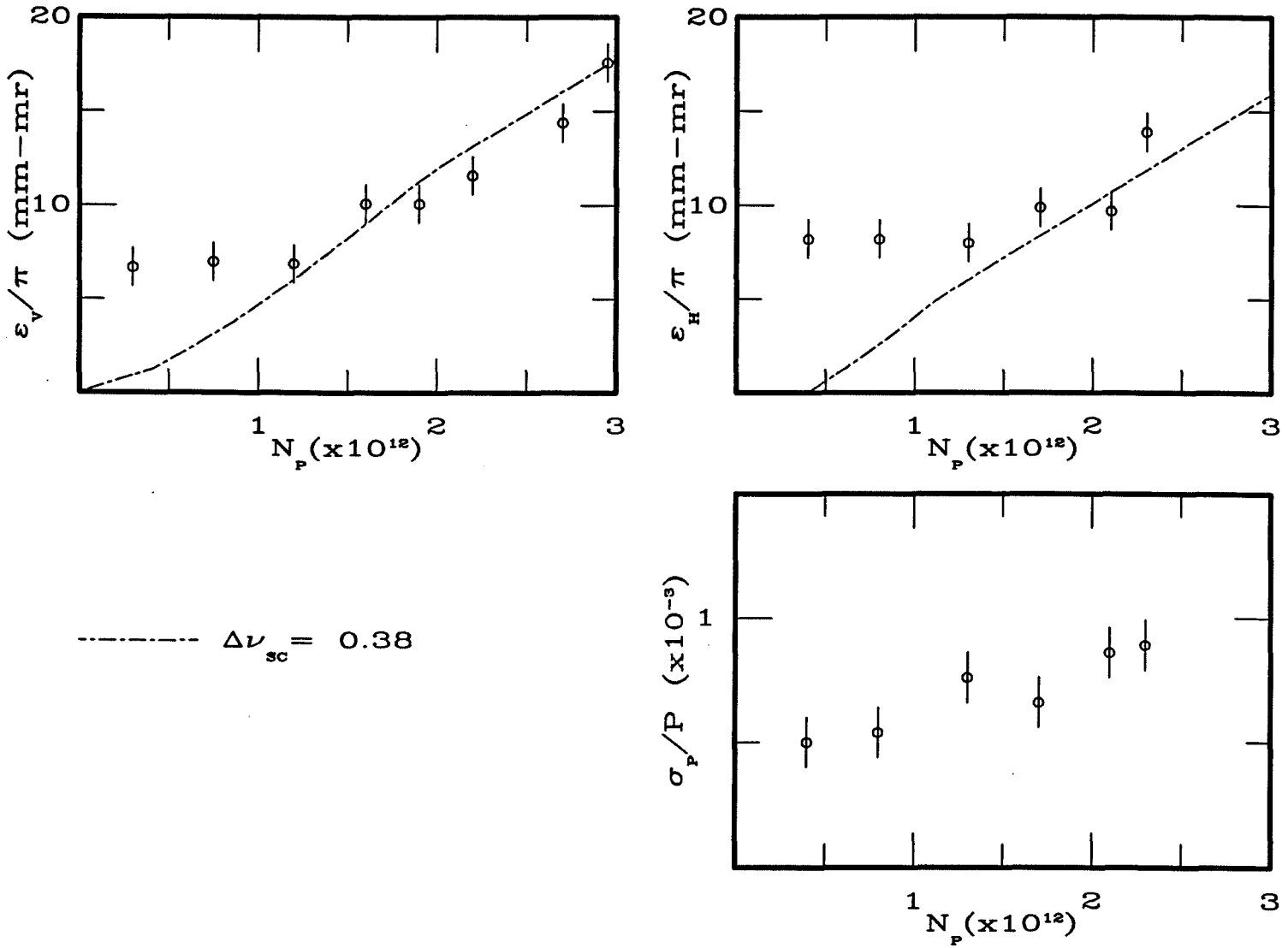

Figure 2 - Booster emittance and momentum spread vs. intensity showing growth at higher intensities.

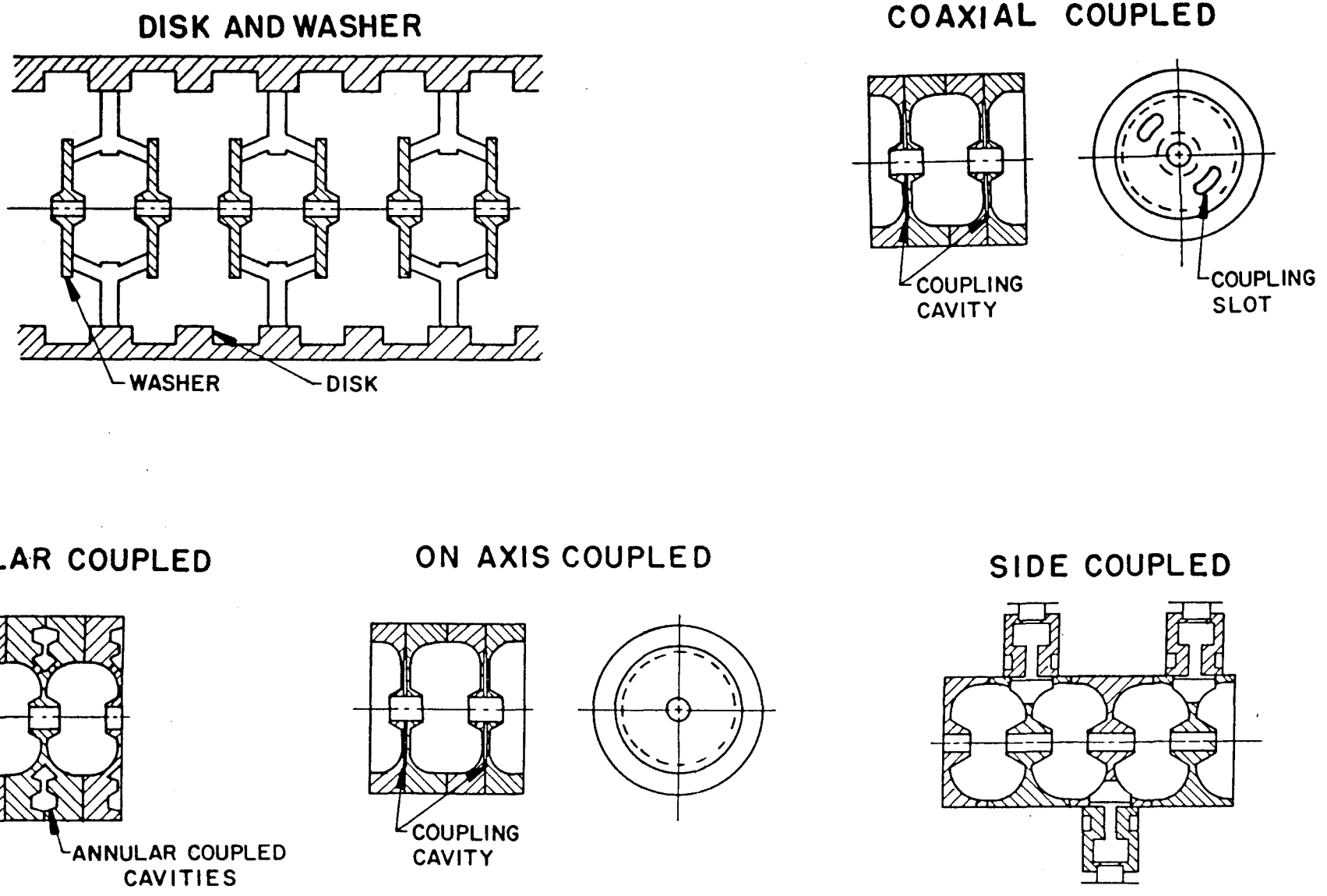

Figure 3 - Five types of standing wave accelerating structures (see Ref. 2)

Figure 4

Disk and Washer (DAW) Linac Structure

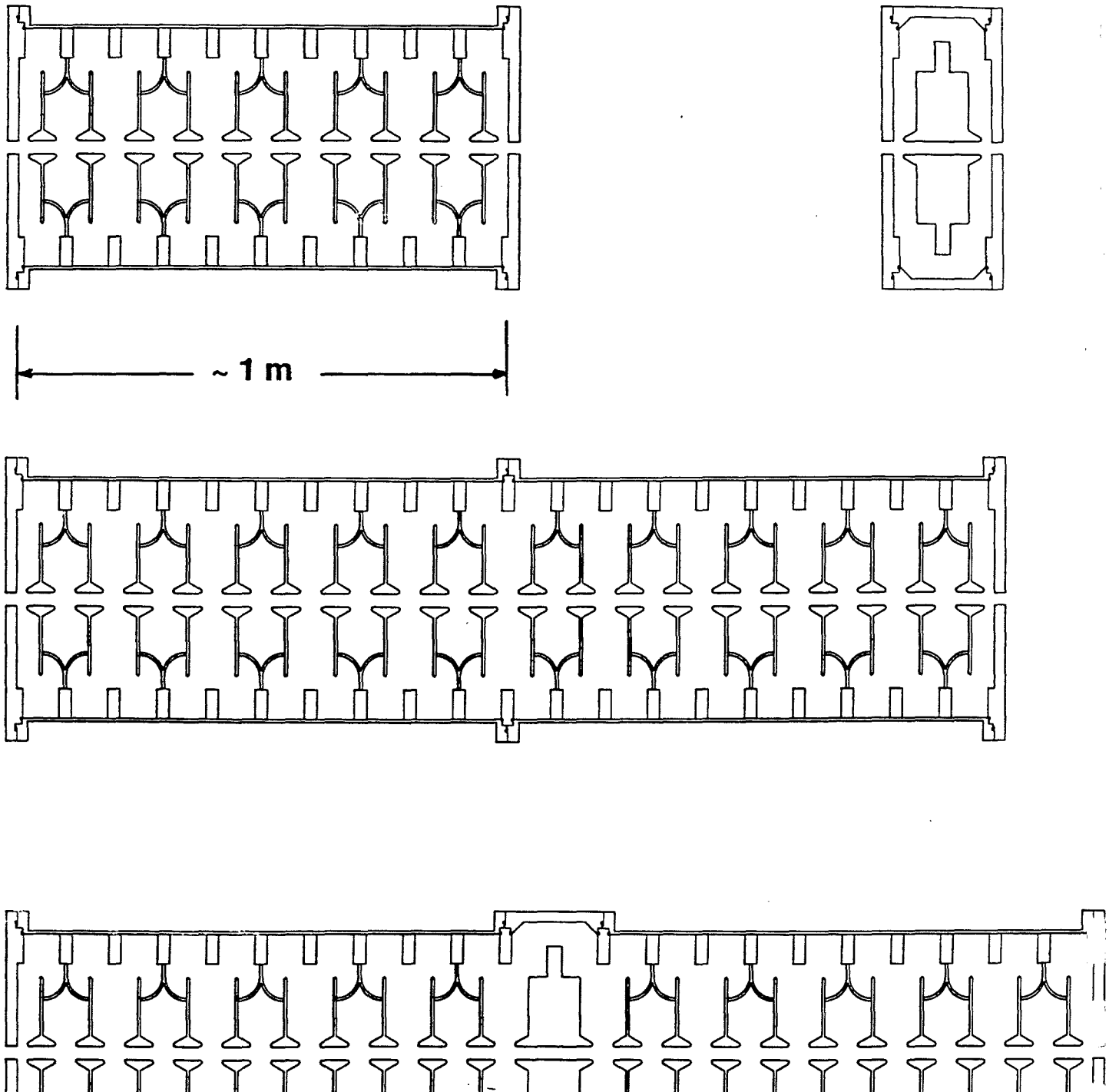

Accelerating Mode Termination

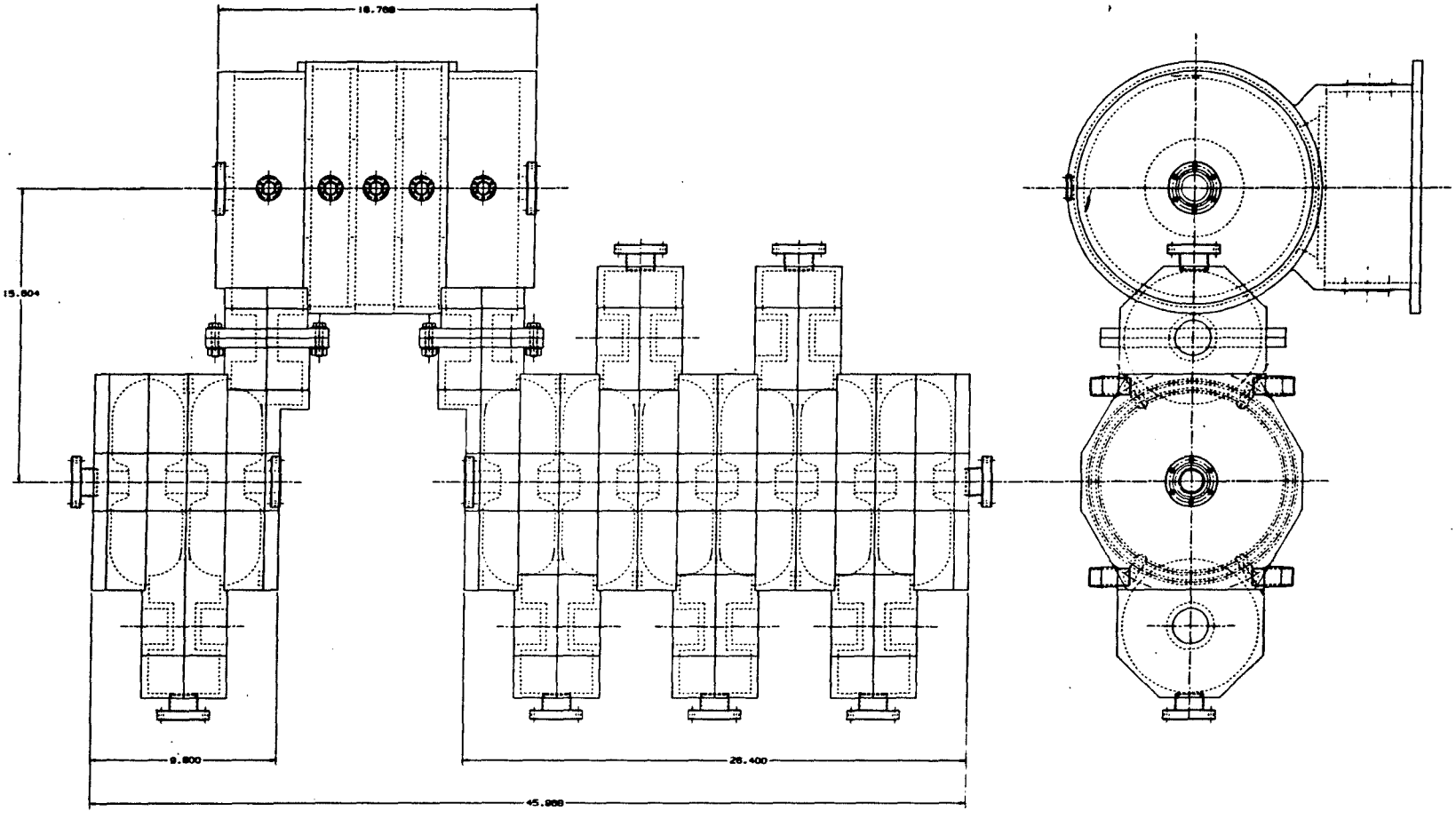

Figure 5 - Side-coupled structure test model

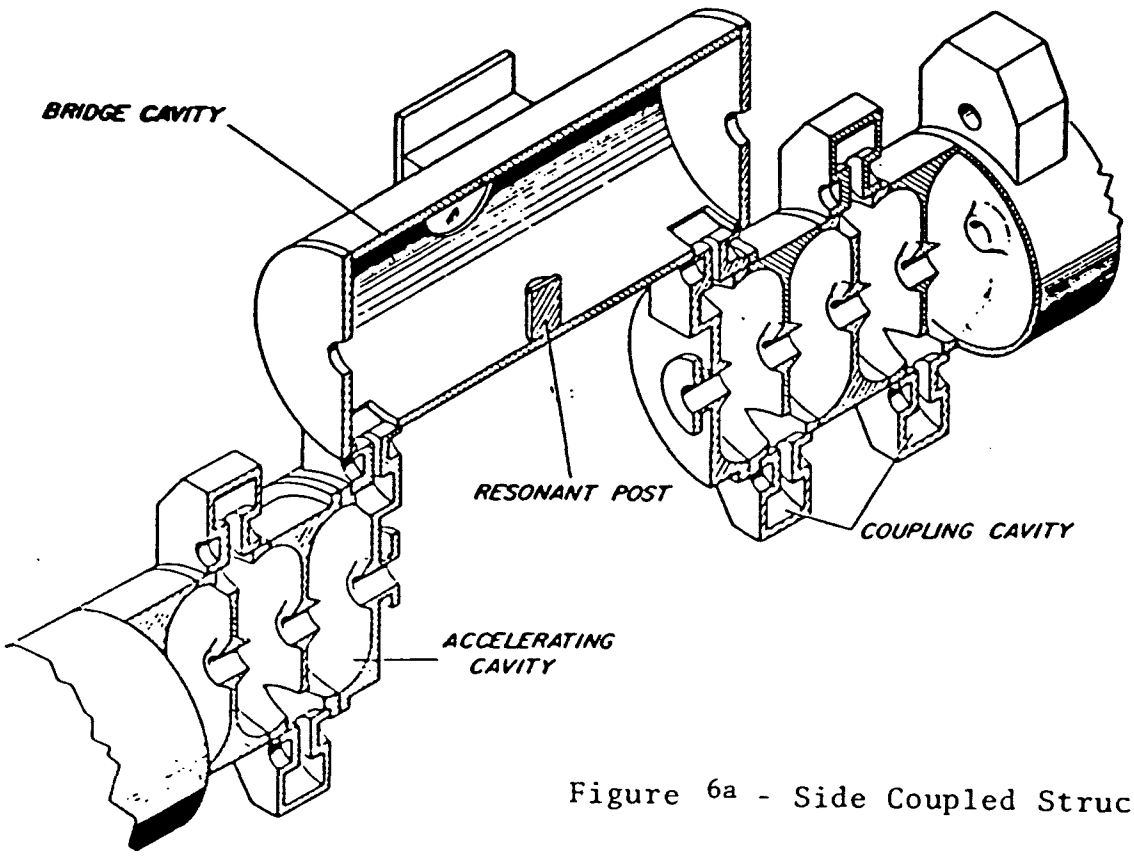

Figure 6a - Side Coupled Structure

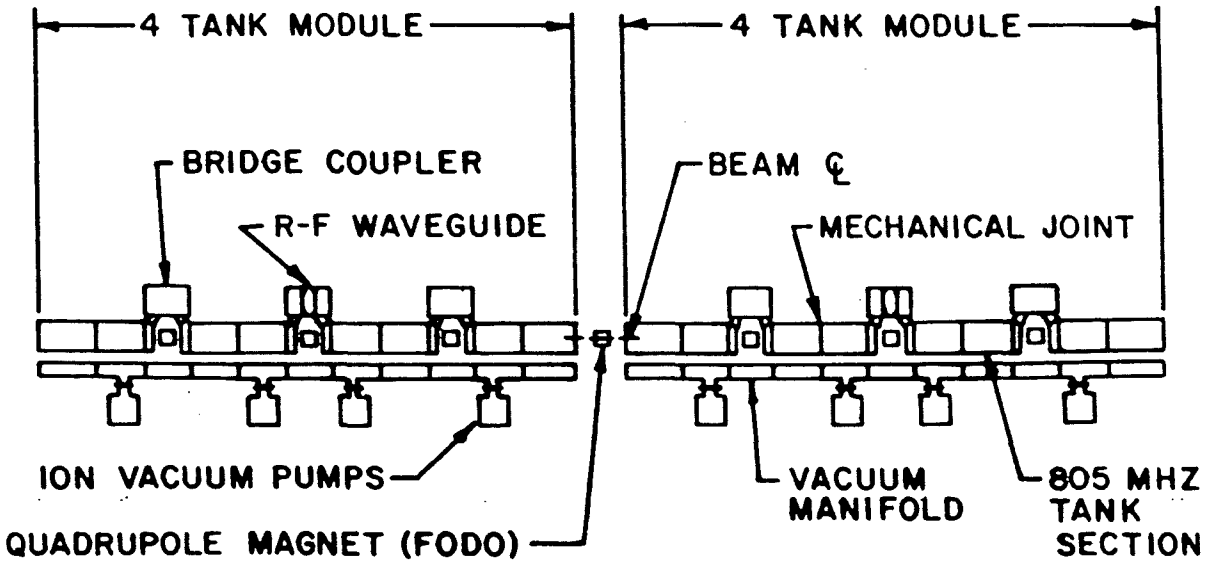

Figure 6b - Schematic of 805 MHz-linac modular sections.

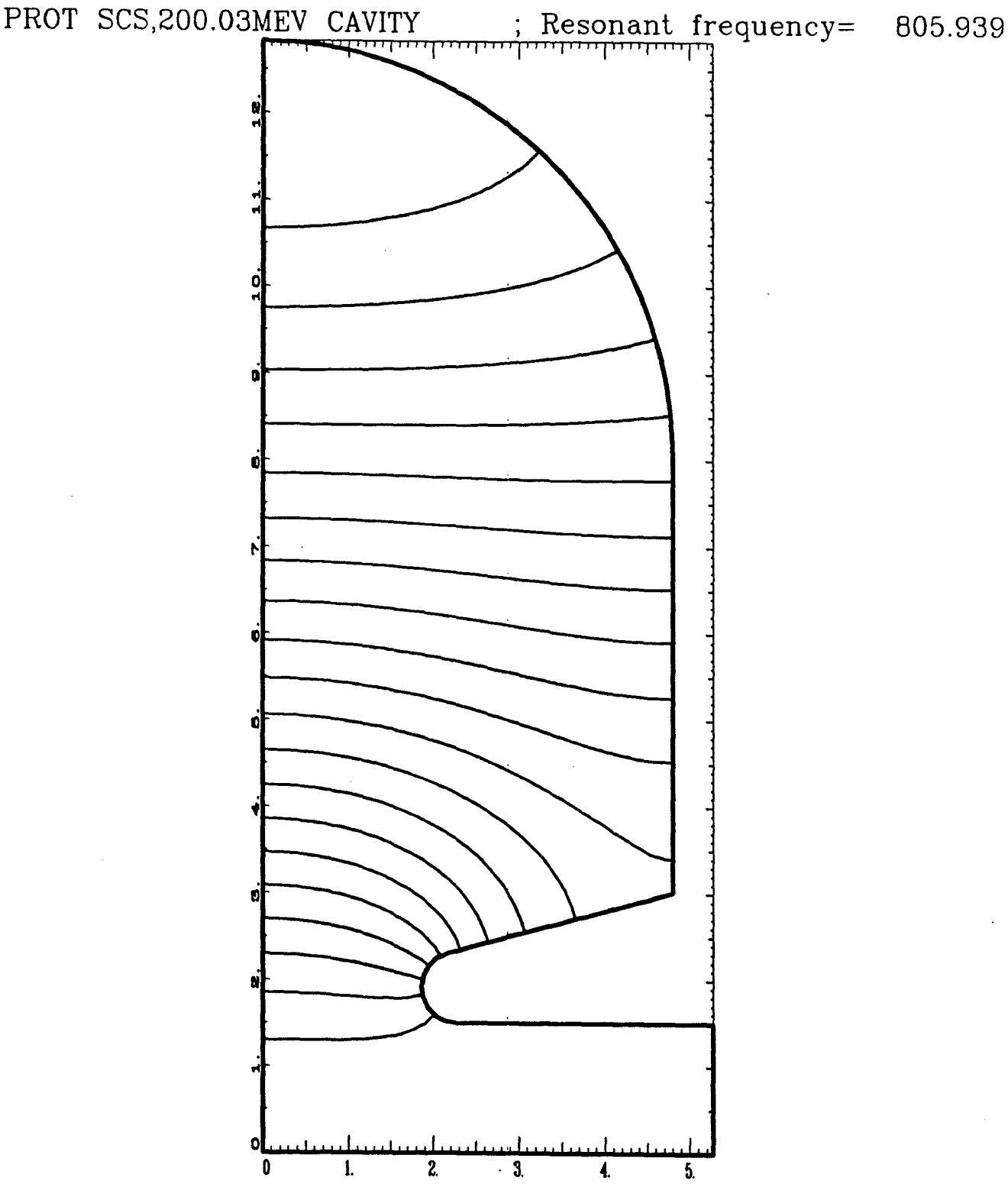

Figure 7 - A quadrant of the accelerating cell for $\beta = 0.5662$ showing the field (actually rH_{ϕ}) as calculated by SUPERFISH.

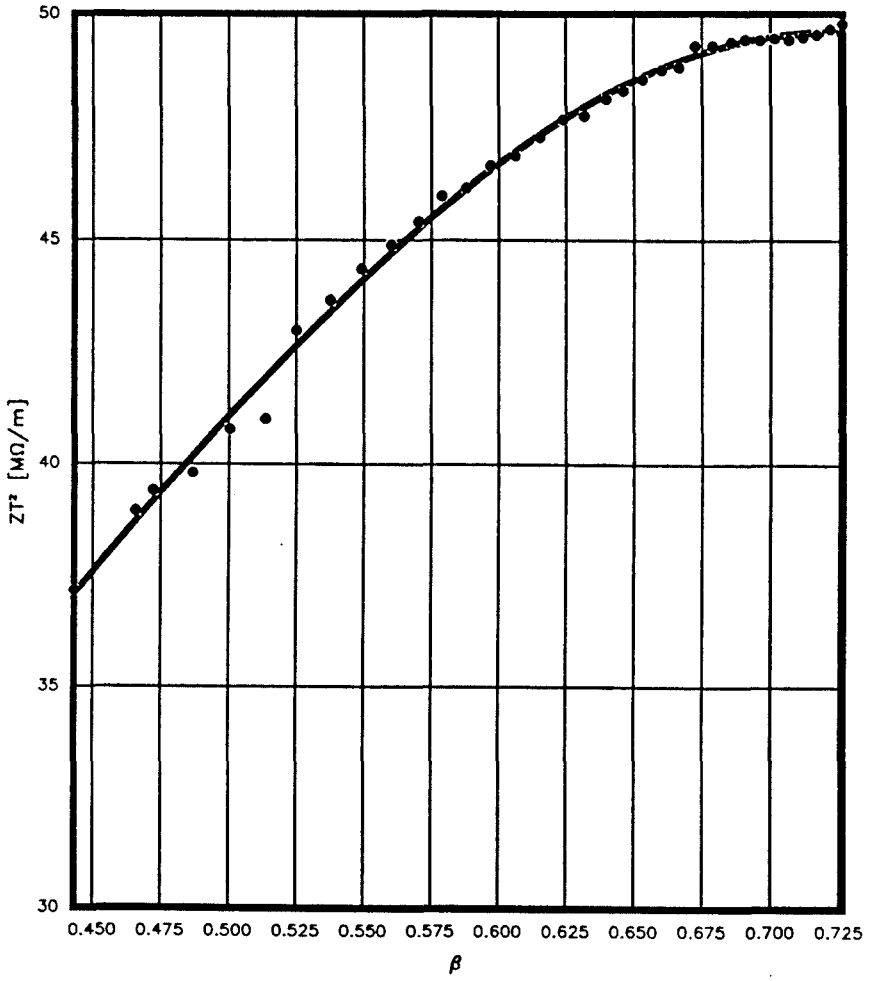

(a)

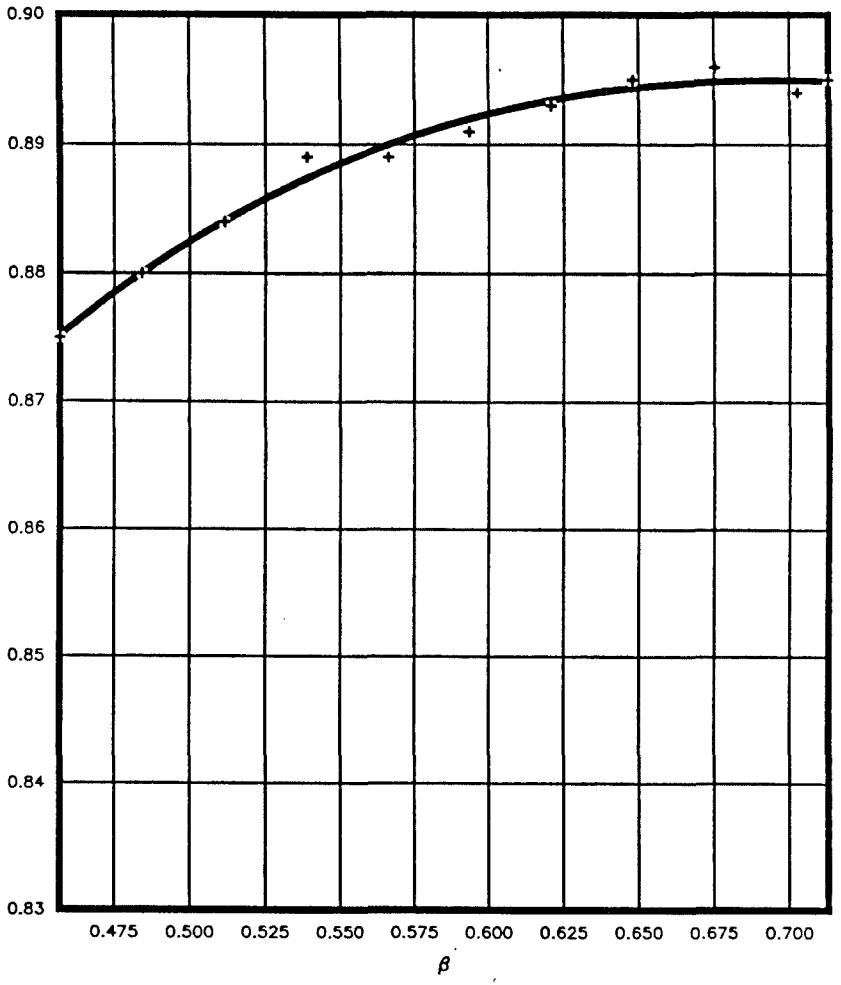

(b)

Figure 8 - Effective shunt impedance ZT^2 (a) and transit time factor T (b) from adjusted SUPERFISH calculations for the SCS plotted as functions of $\beta=v/c$ for the energy range 116 to 400 MeV.

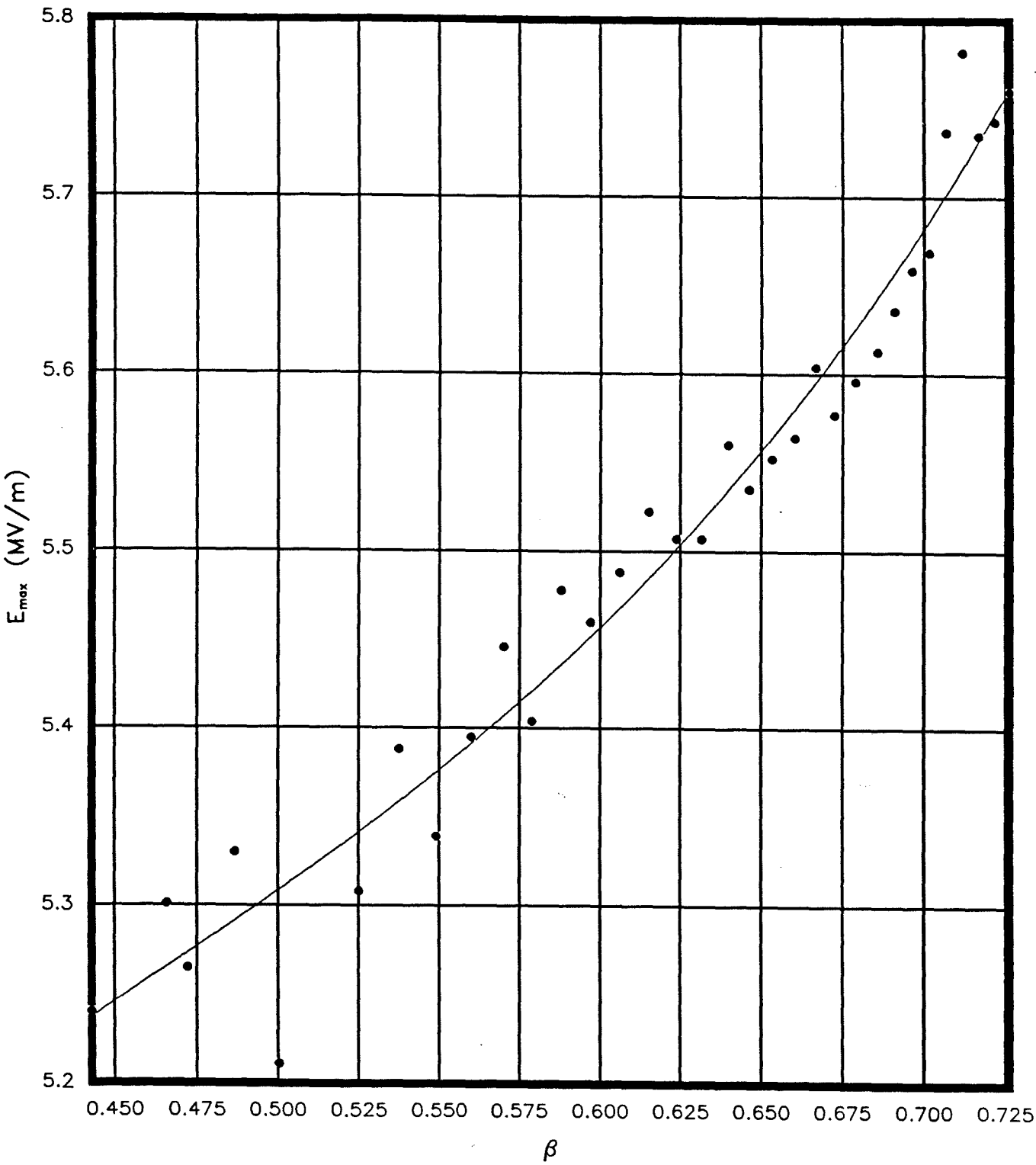

Figure 9 - Maximum surface gradient E_{max} for SCS when the average axial gradient E_o is 1 MV/m plotted vs. $\beta = v/c$ for the energy range 116 to 400 MeV.

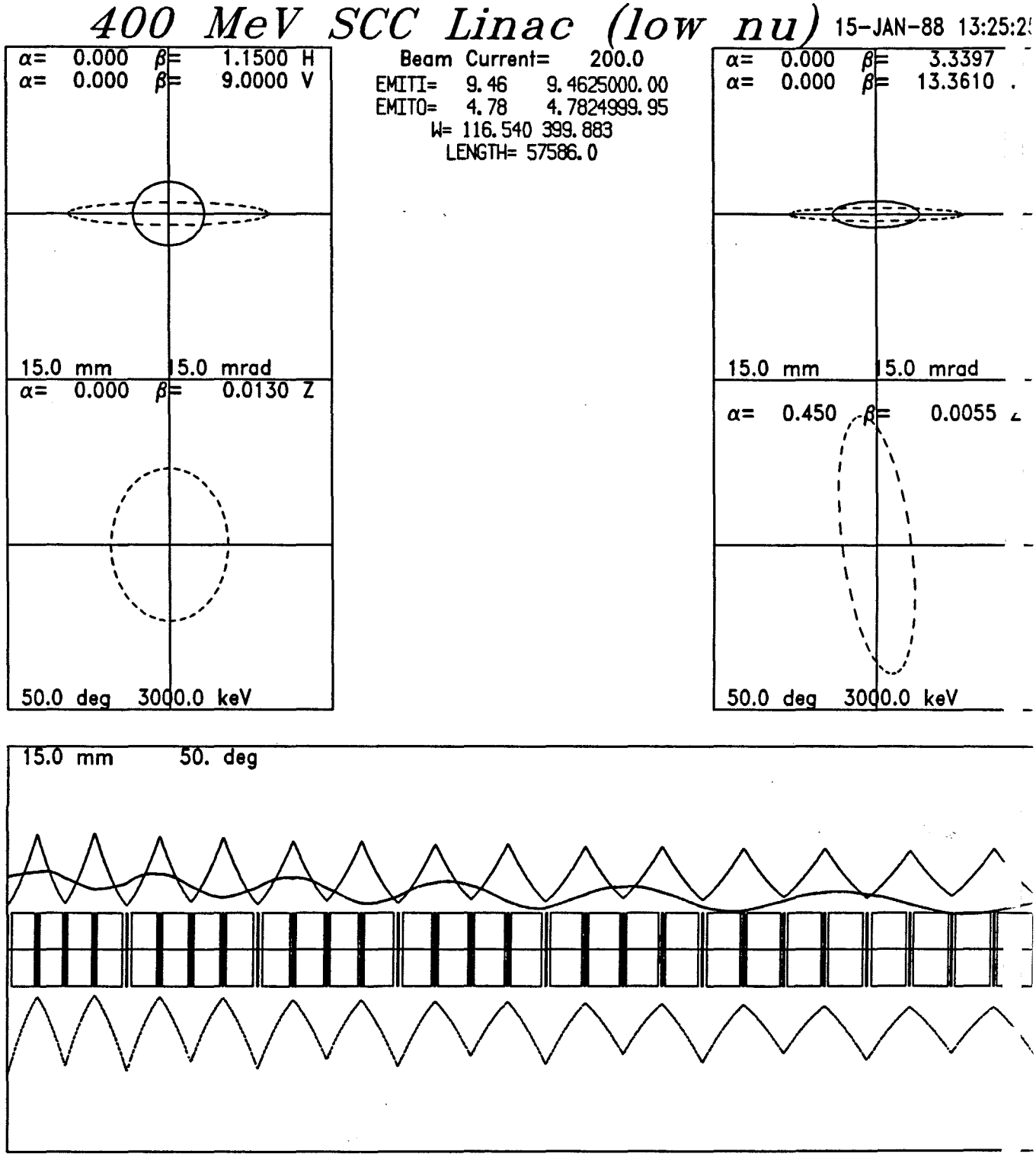

Figure 10 - Beam envelopes, initial beam ellipses, and final beam ellipses for the 400-MeV linac. The envelopes contain $\sqrt{5}$ σ or about 90% of the beam. In the envelope trace the horizontal and longitudinal envelopes are shown above the tank layout, the vertical plane envelope is below.

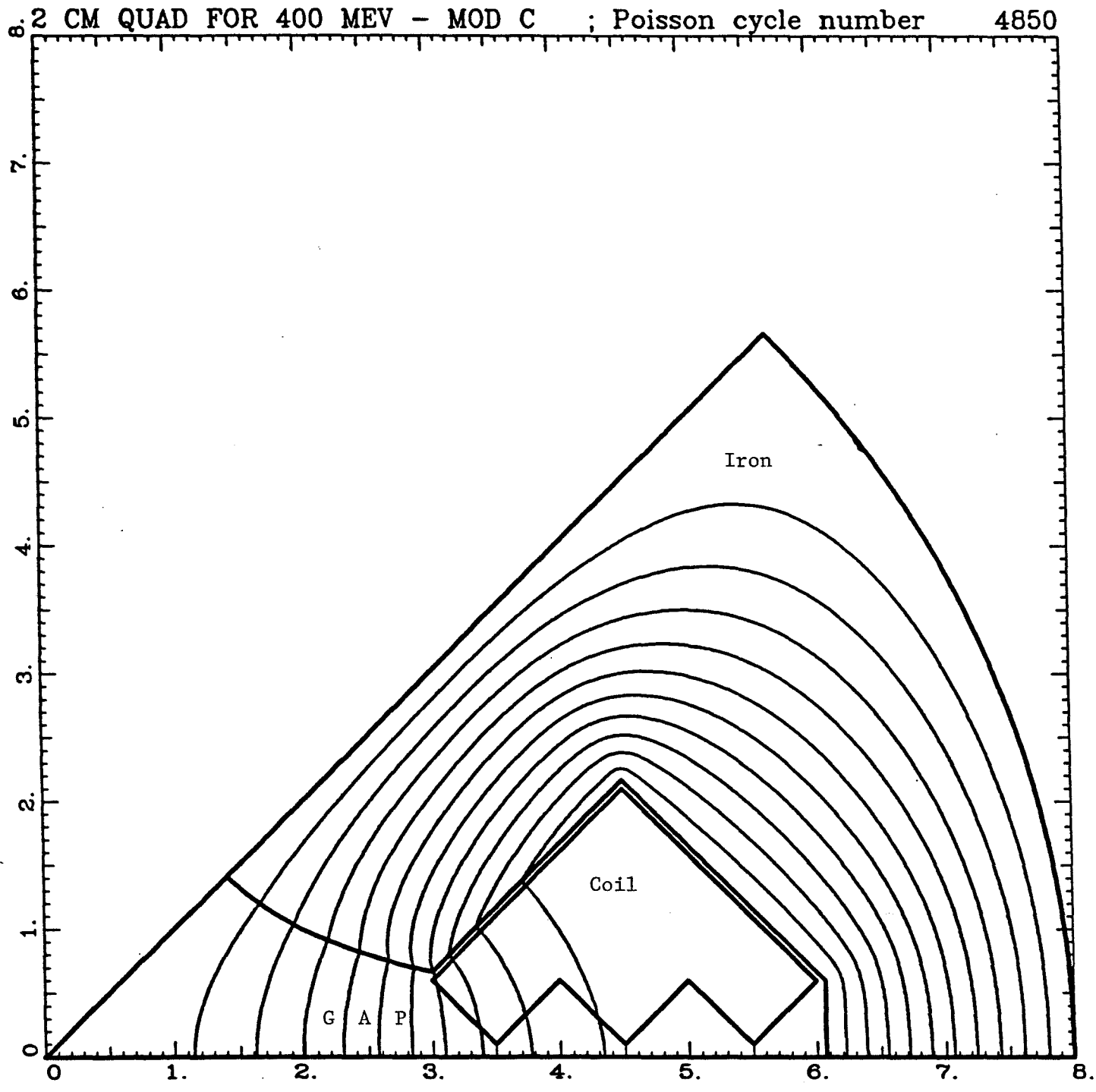

Figure 11 - Output of the program POISSON showning an octant of an 8 cm (1) quad with 2 cm pole tip radius suitable for installation in the bridge couplers.

805 MHz SCS RF System

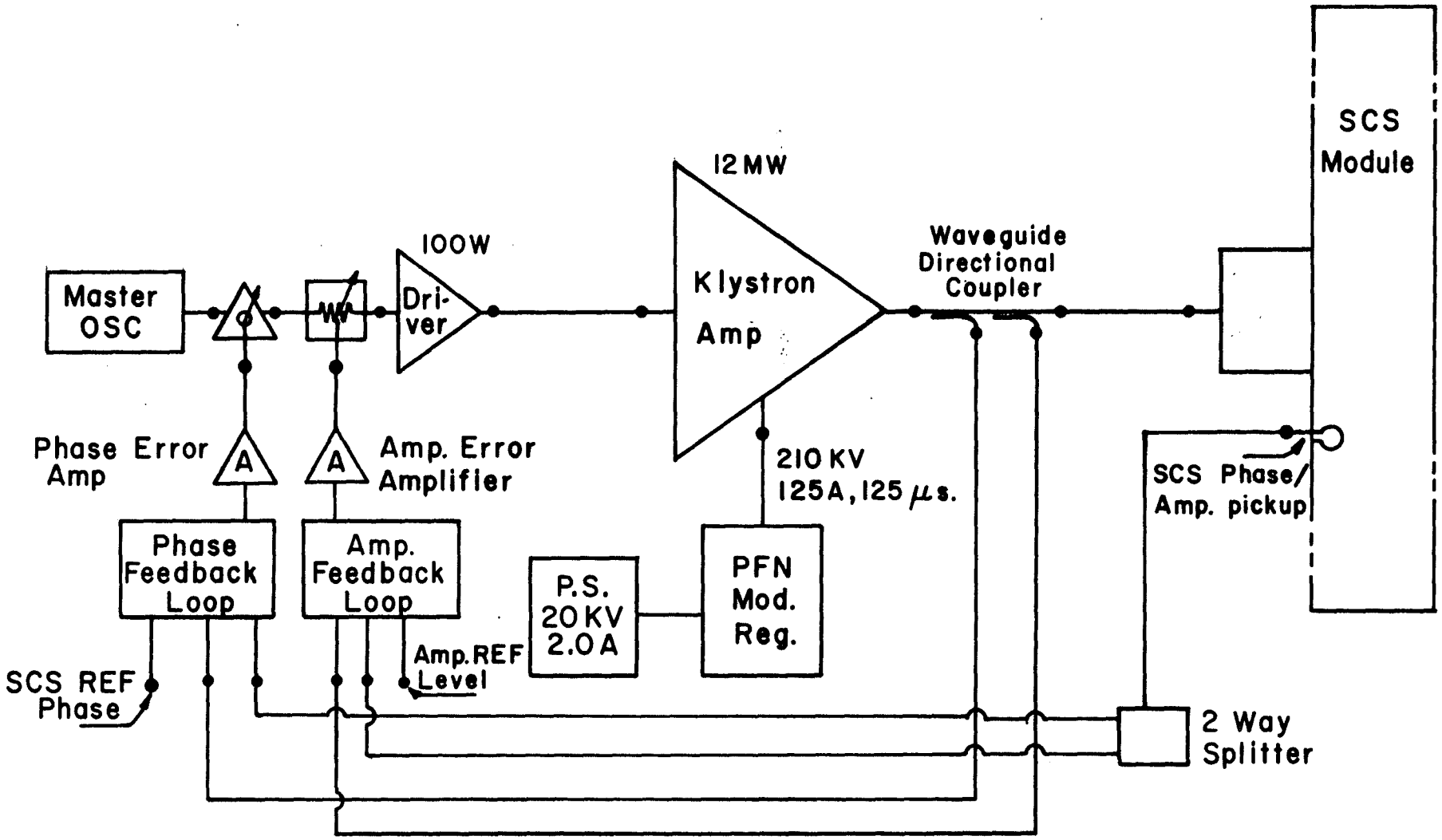

Figure 12

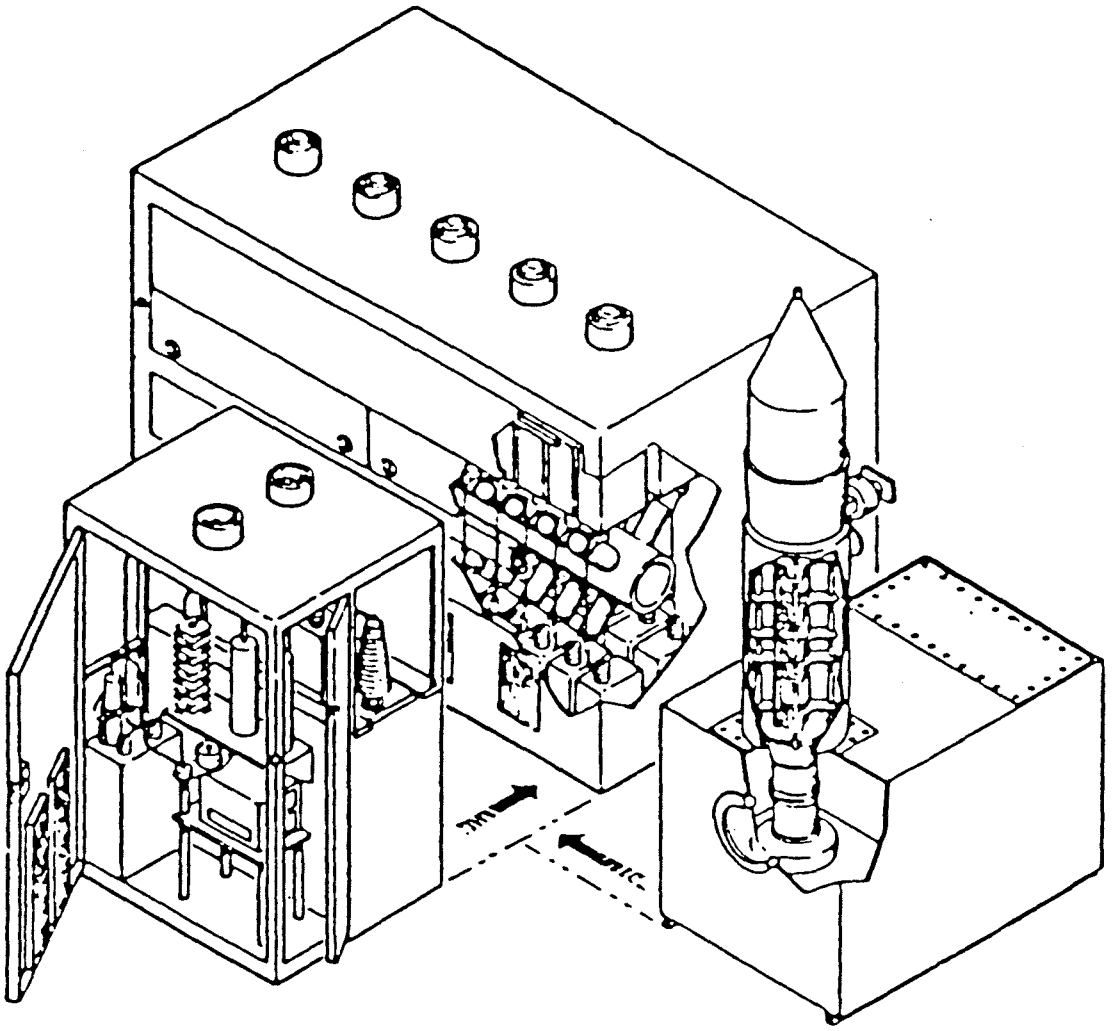

Figure 13 - Pictorial Assembly of
Klystron Power Supply

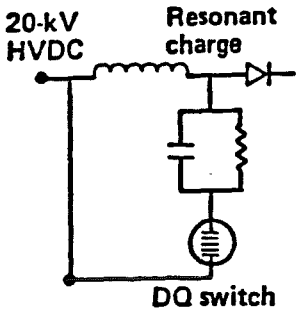

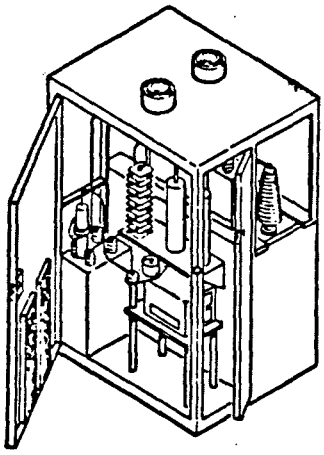

Conditions:
- Resonant charge: 20 ms
- Regulation: 0.5%

FIGURE 14. REGULATOR CIRCUIT

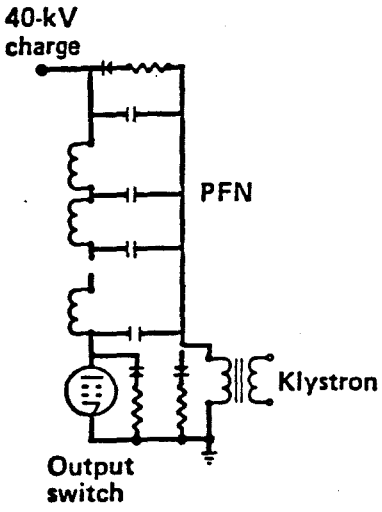

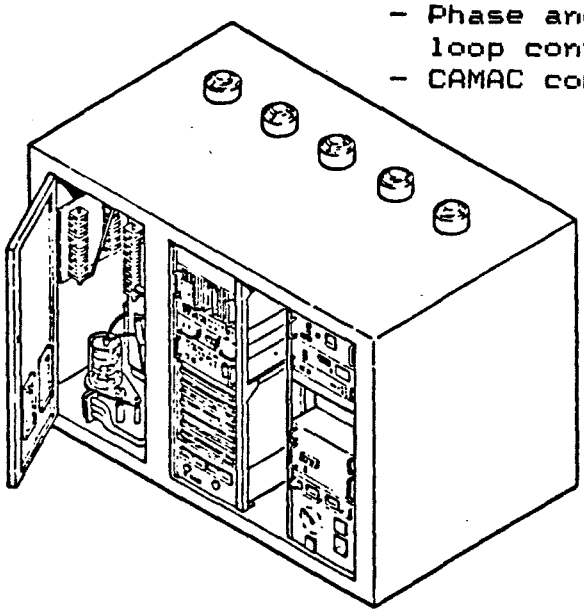

Conditions:
- 125 micro sec line
- 27 MW maximum output
- Phase and amplitude loop control
- CAMAC computer link

FIGURE 15. MODULATOR CIRCUIT

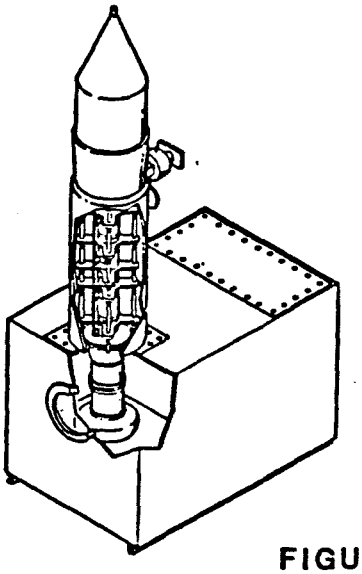

Conditions:
805 MHZ Klystron
- 12 MW peak, 125 micro sec
- 22.5 KW average

FIGURE 16. KLYSTRON AND PULSE TRANSFORMER CIRCUIT

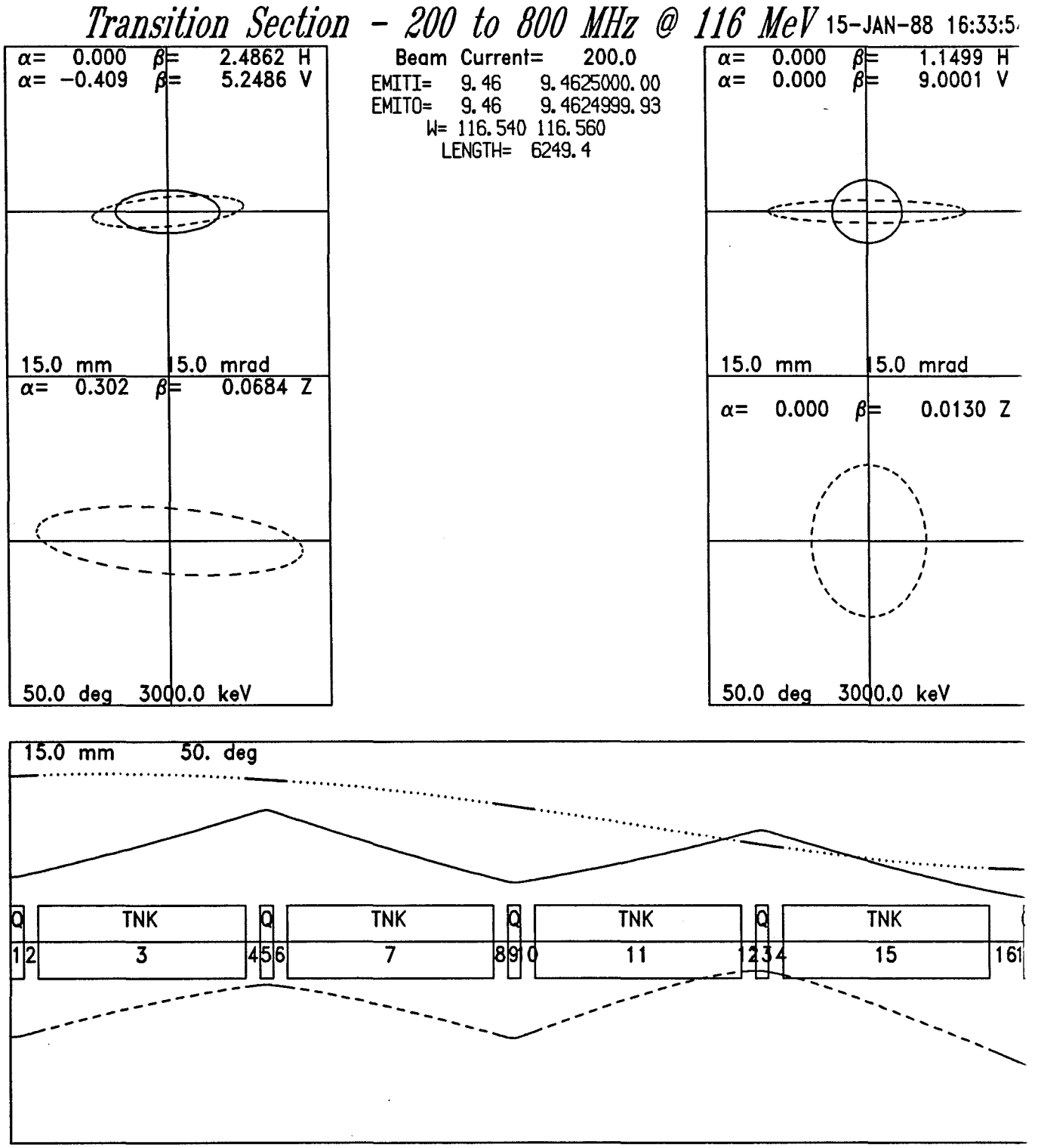

Figure 17 - Initial beam ellipses, final beam ellipses and beam envelopes for the 116-MeV transition section. The bunch width and horizontal plane envelope are shown above the layout schematic; the vertical plane envelope is shown below the layout.

FIGURE 18. BUNCH SIZE REDUCTION AND SHAPE OSCILLATIONS.

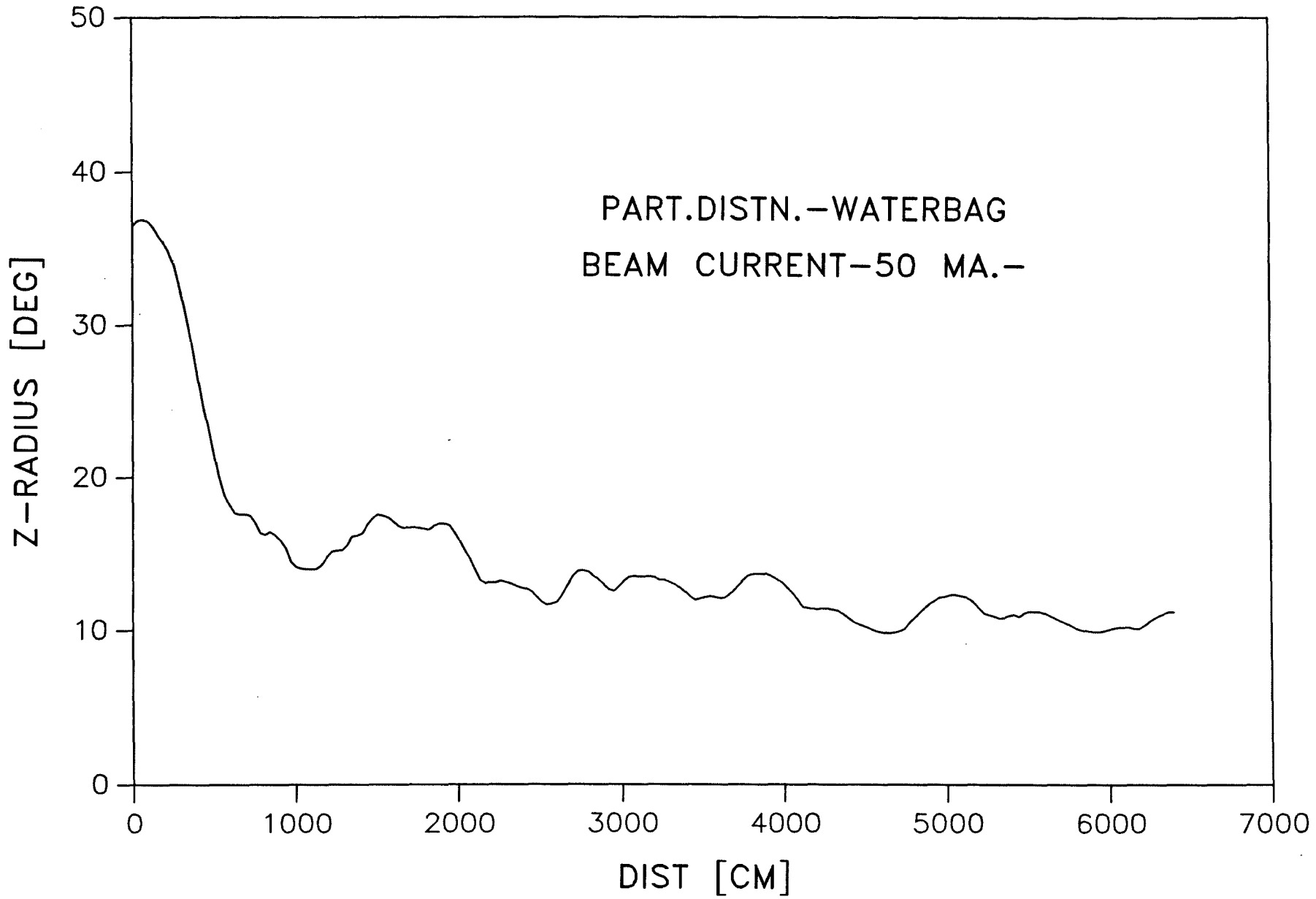

FIGURE 19. Z-PLANE RMS EMITTANCE GROWTH (116-400 MEV)

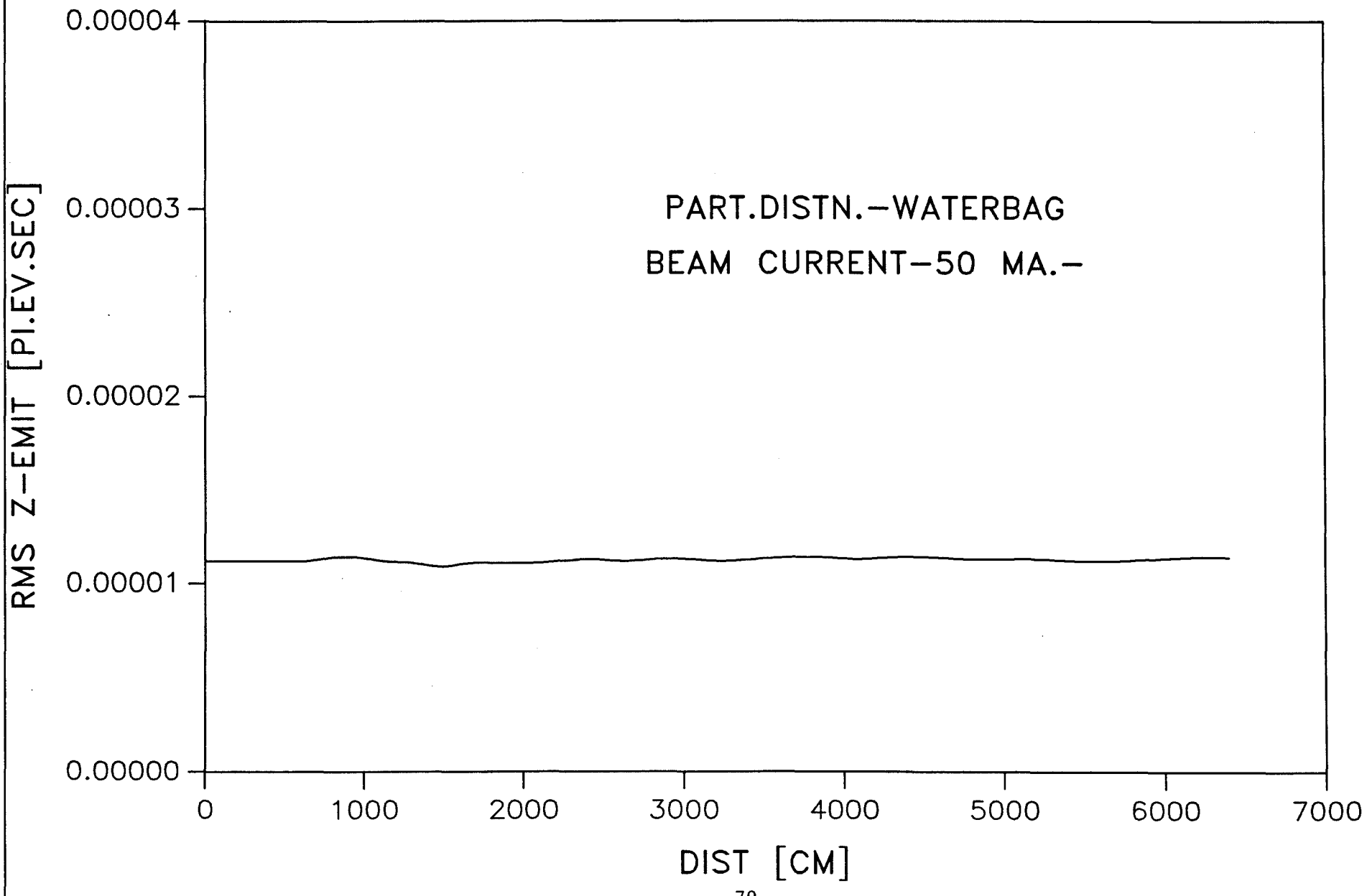

FIGURE 20. BEAM RADIUS IN FODO CHANNEL (116–400 MEV)

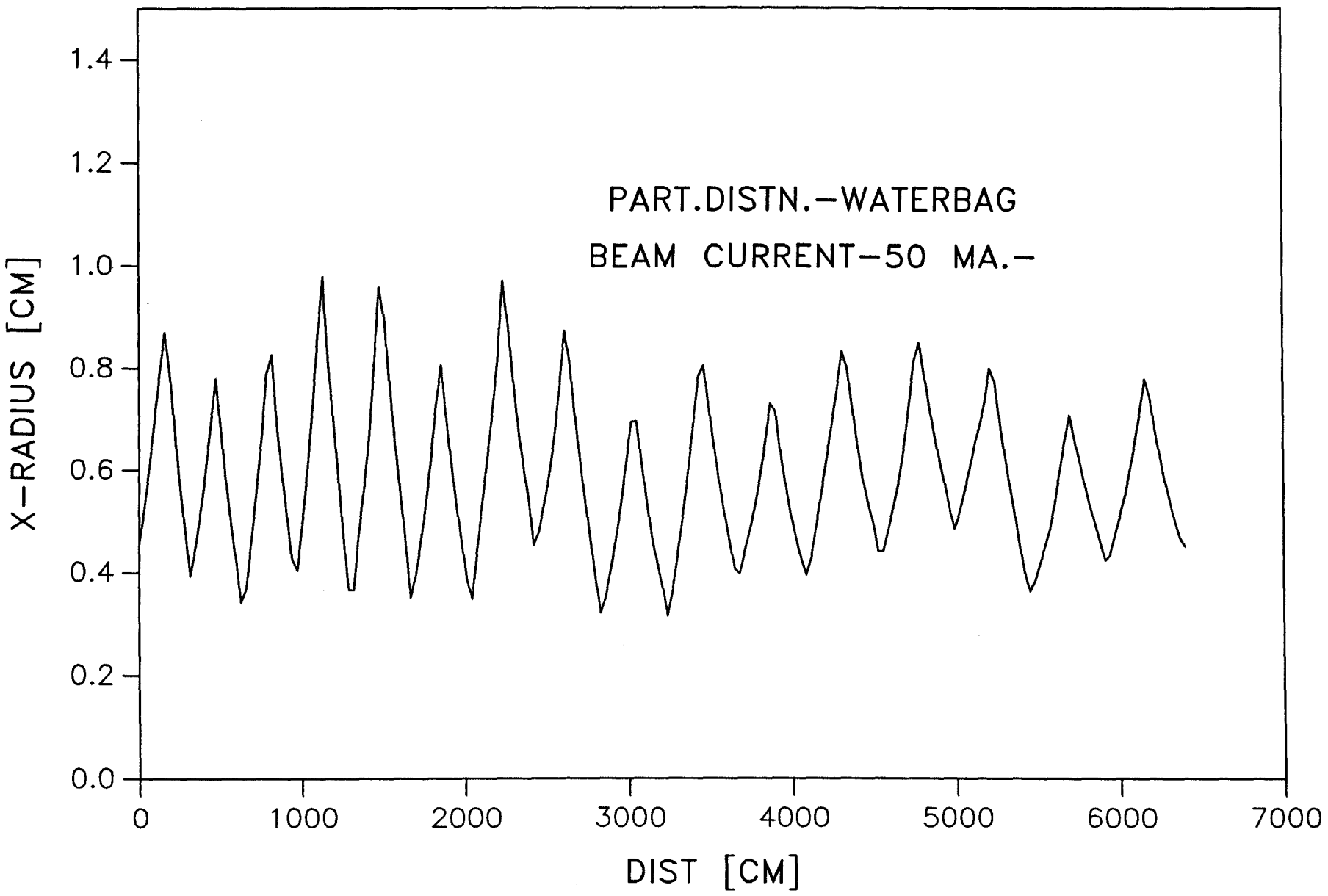

FIGURE 21. X-PLANE RMS EMITTANCE GROWTH (116-400 MEV)

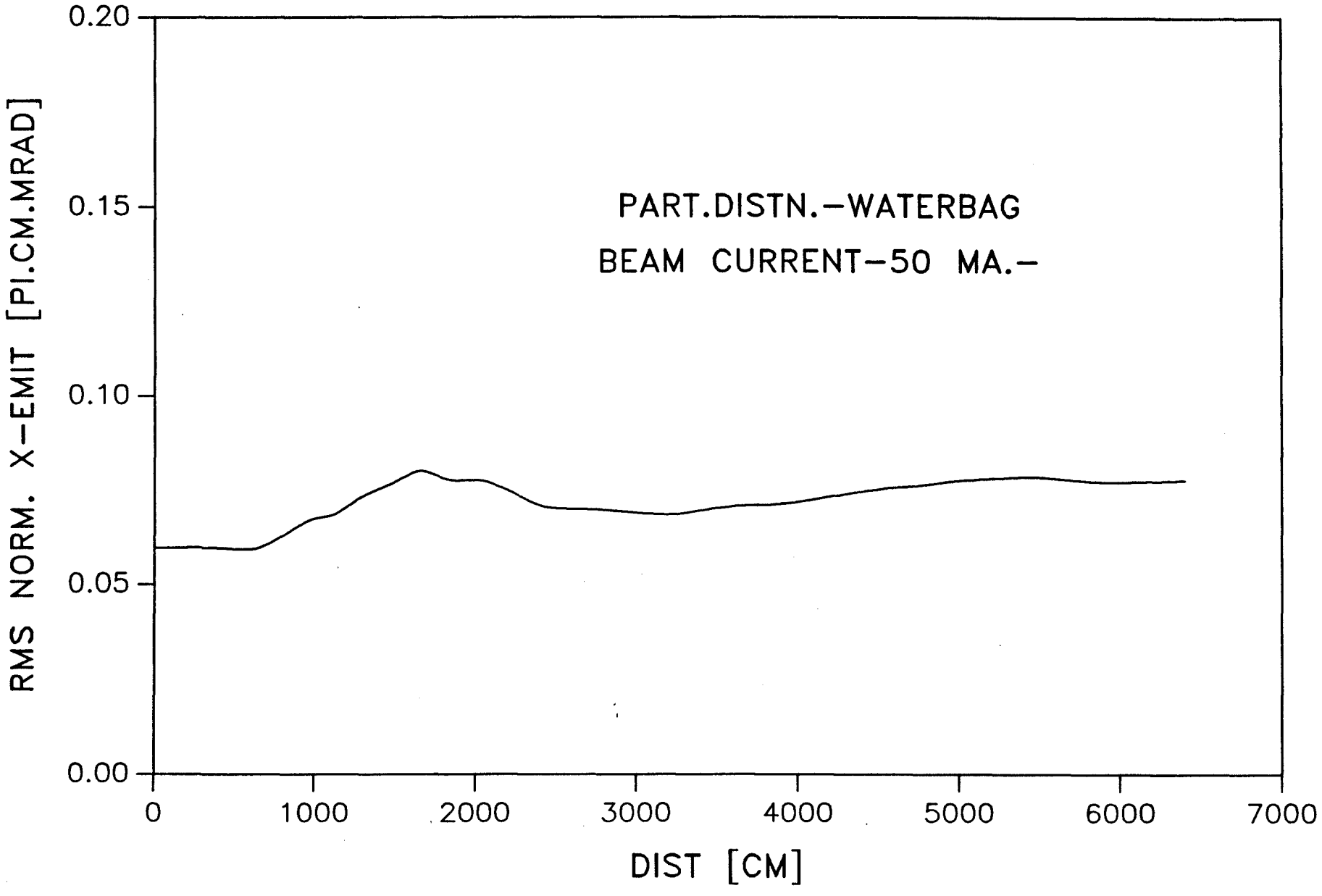

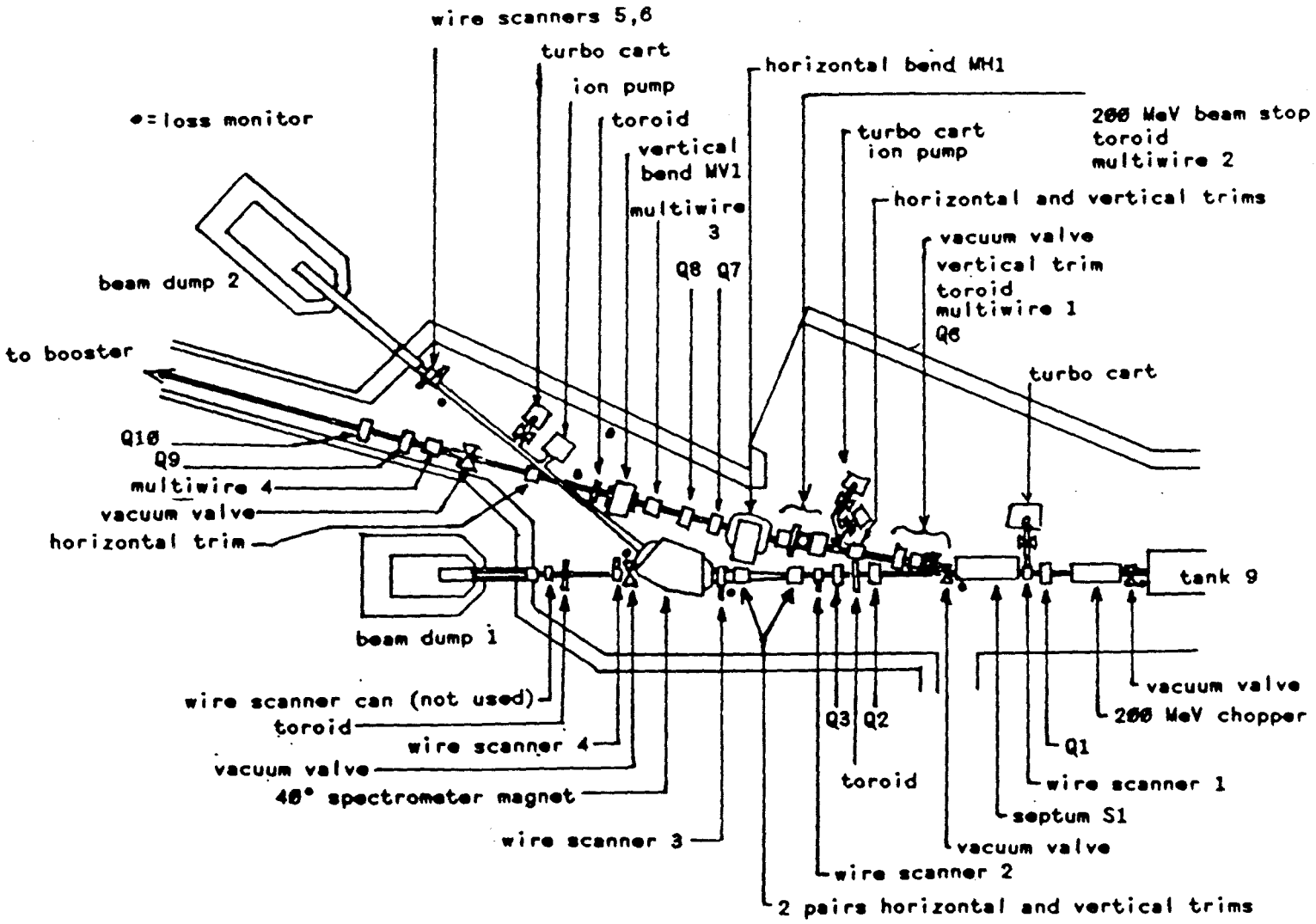

Figure 22 - Current 200-MeV Area

Figure 23 - Present 200-MeV Transfer Line to Booster with elements to be modified in boxes.

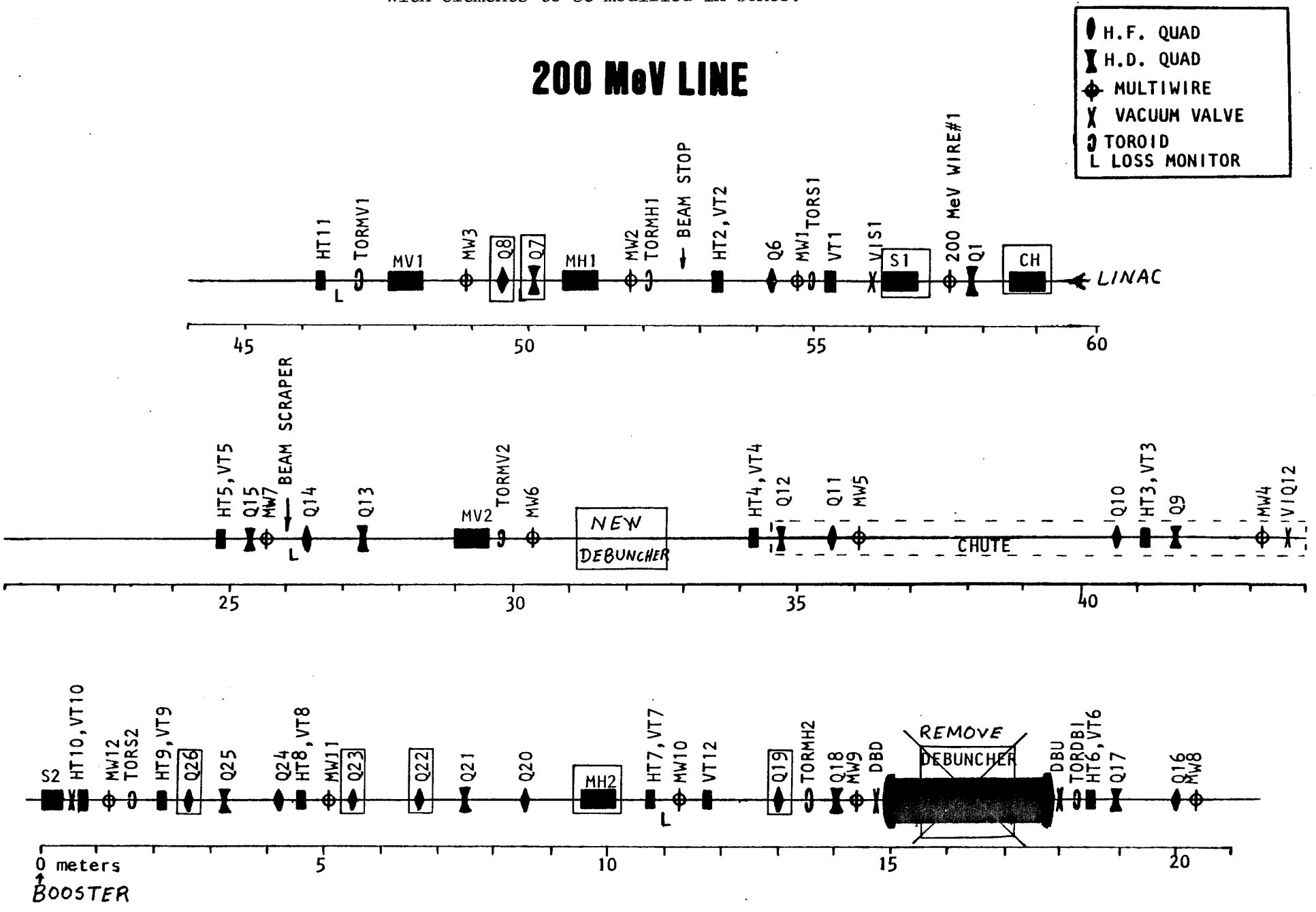

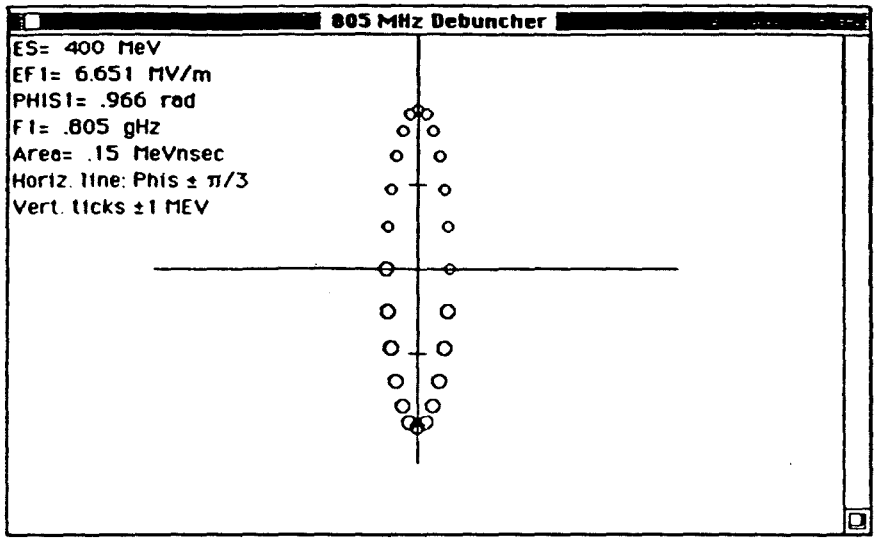

(a)

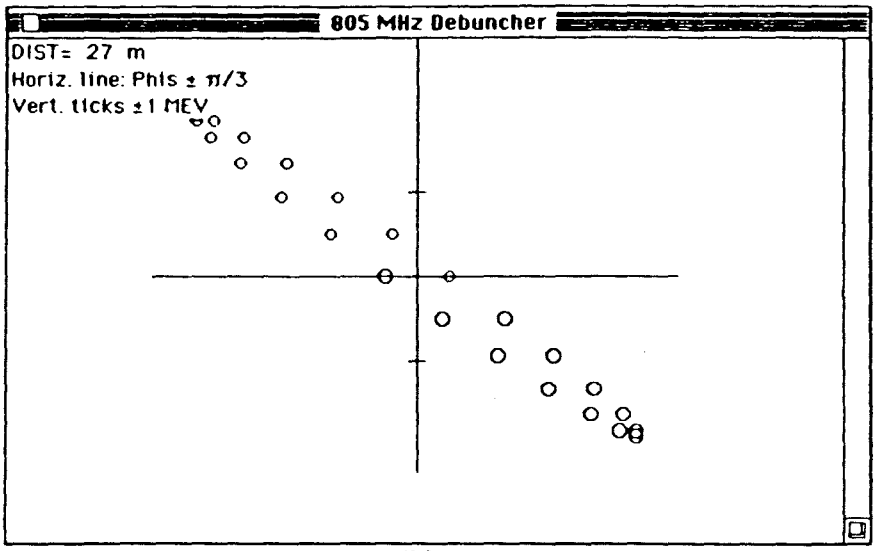

(b)

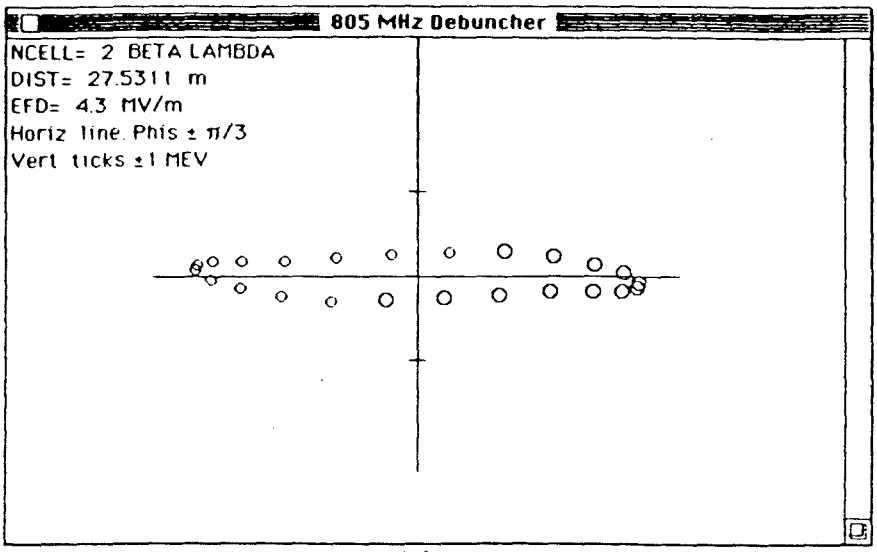

(c)

Figure 24 - Phase Space Simulation for 805 MHz Debuncher.

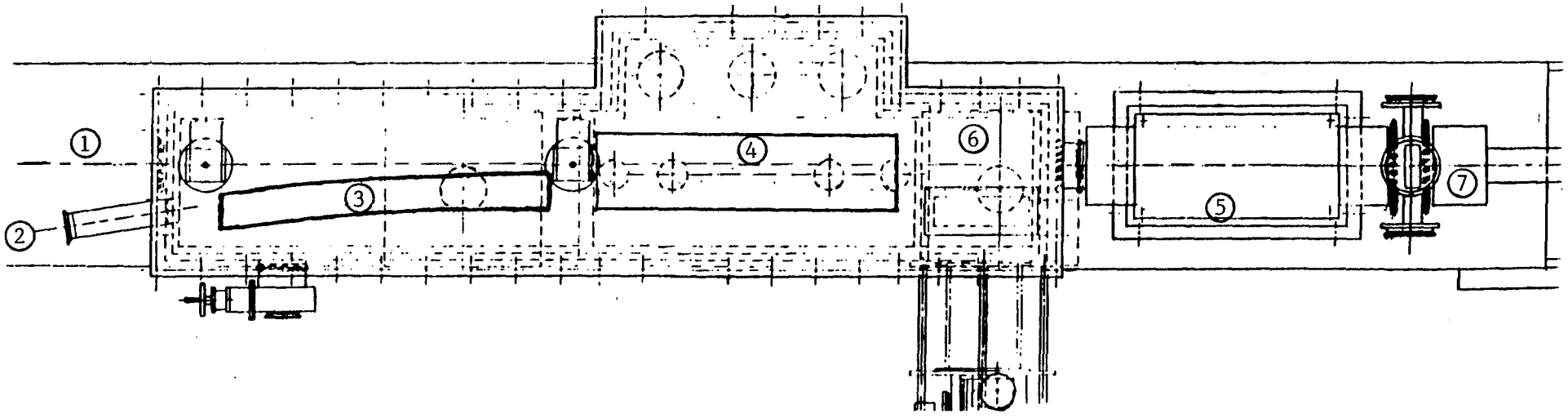

Figure 25 - The present H^- charge-exchange injection system in the Booster. The numbers in the figure correspond to:

1: Normal closed orbit
2: Incoming H^- beam
3: Current-sheet septum magnet
4,5: Orbit-bump magnets
6: Foil-changing mechanism
7: Beam position pickup and correction element package

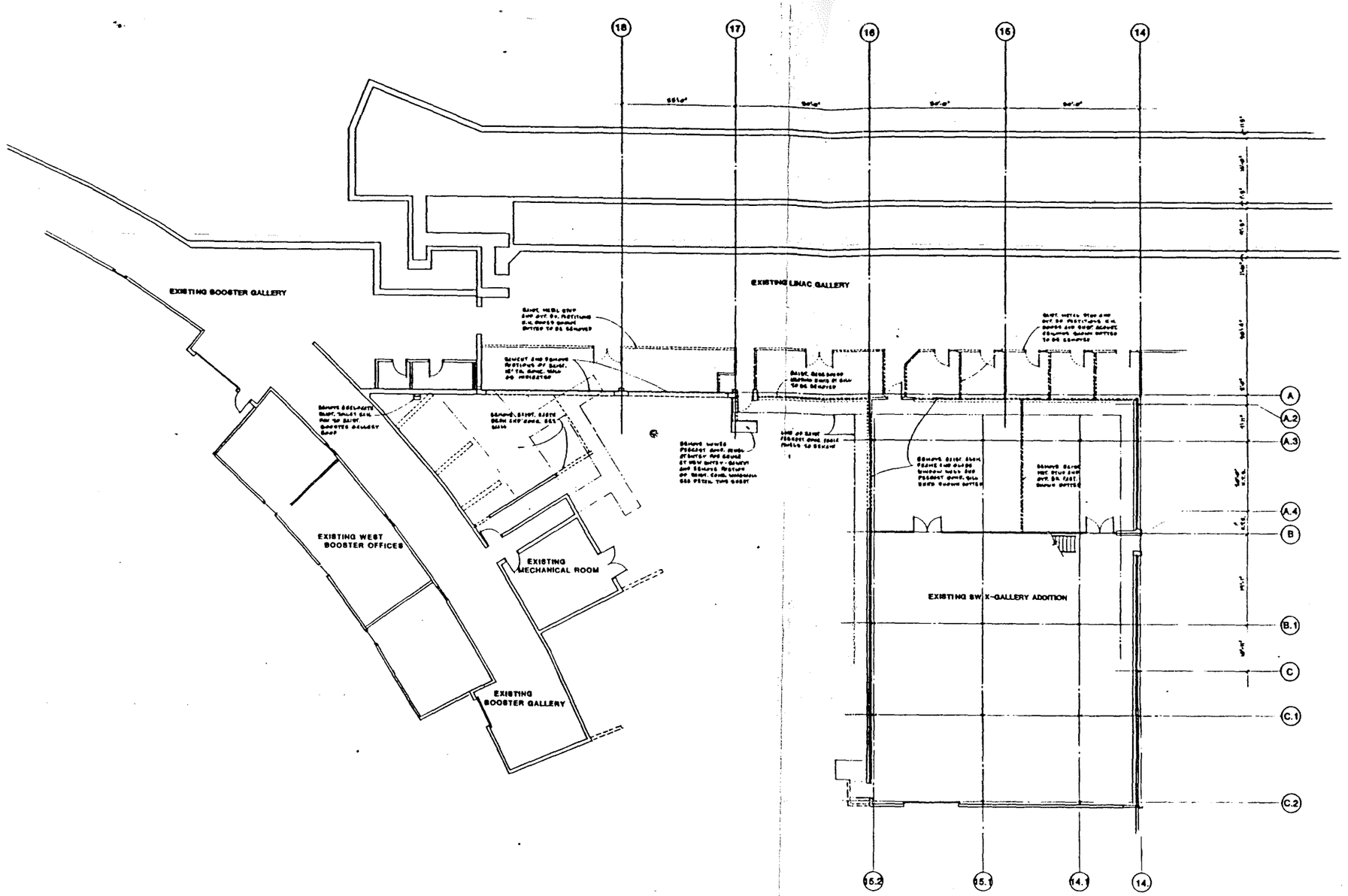

DEMOLITION PLAN

Figure 26

Demolition Plan of Existing Structures

SCALE

FERMI NATIONAL ACCELERATOR LABORATORY

400 MEV LINAC UPGRADE

DEMOLITION PLAN

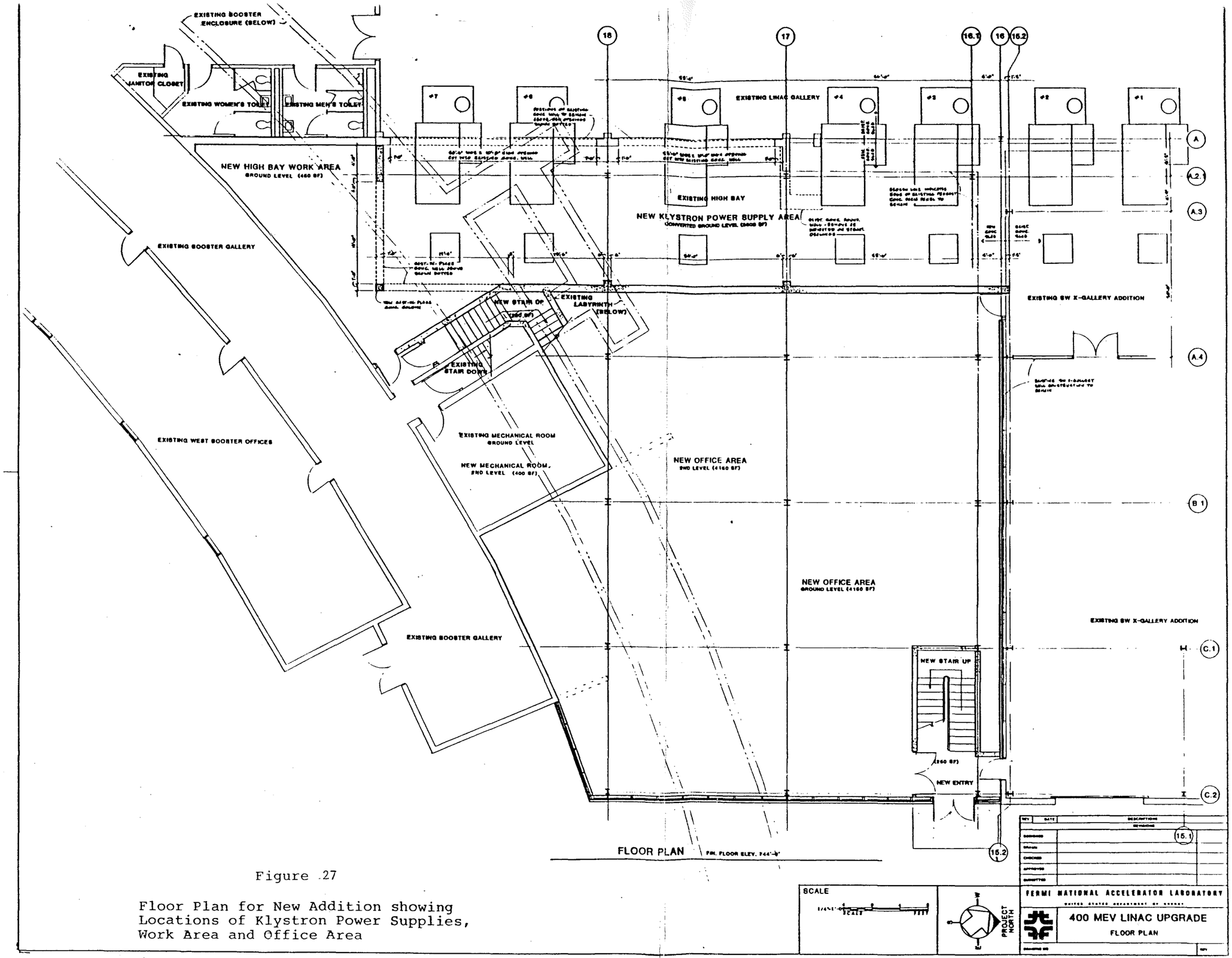

Figure 27

Floor Plan for New Addition showing Locations of Klystron Power Supplies, Work Area and Office Area

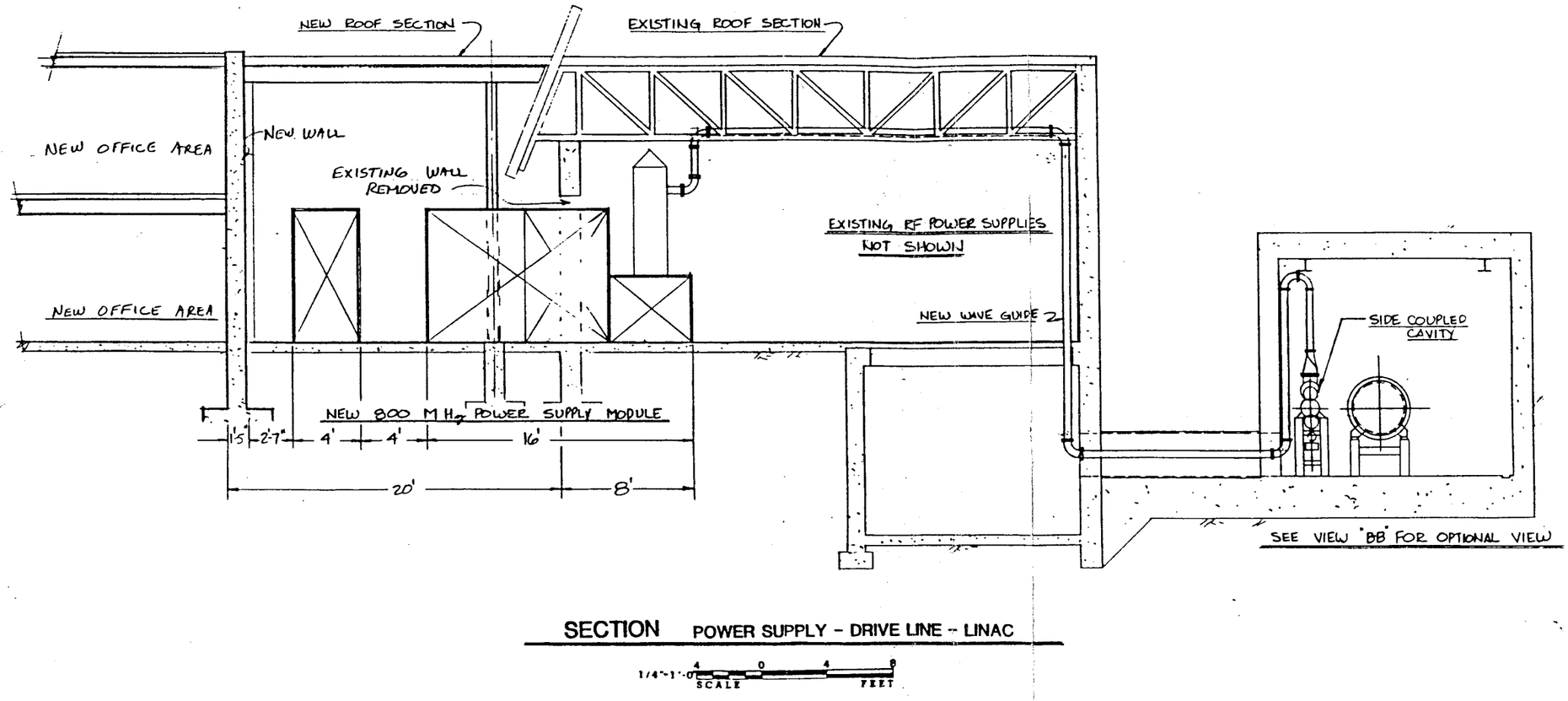

SECTION POWER SUPPLY - DRIVE LINE -- LINAC

1/4"=1'-0" SCALE 4 0 4 8 FEET

Figure 28

Elevation Section showing the SCS Module Installation in the Linac Enclosure and the 800 Mhz RF Drive Line from the Klystron Power Supply

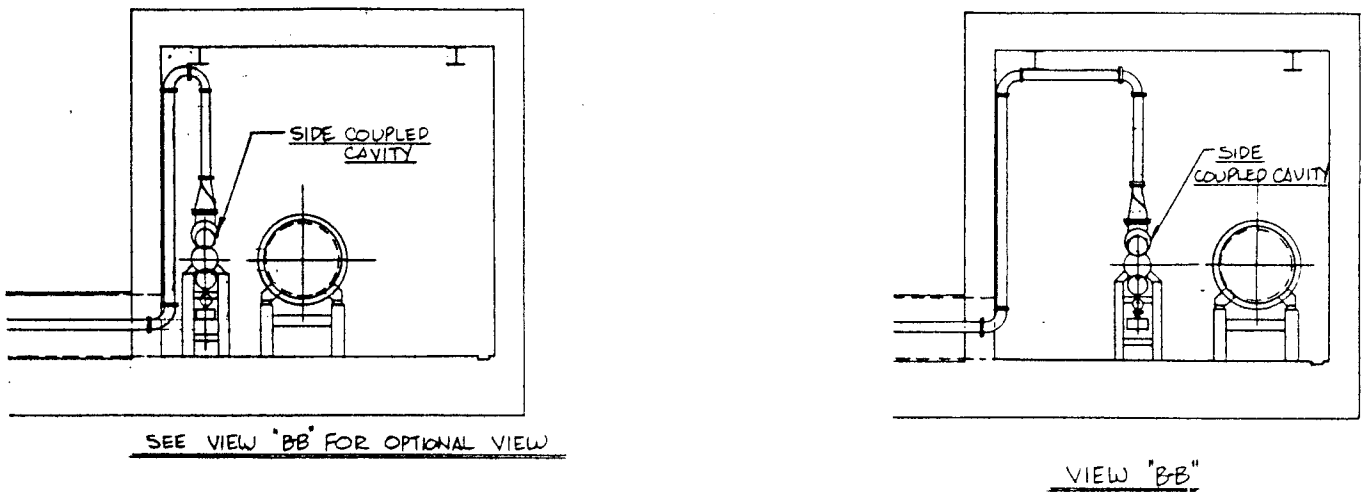

Figure 29 - Location for SC Module Off-line (left) or In-line (right).